Modeling of DFIG Based Wind Turbine Mitigating Dynamic Behavior under Varying Load and Asymmetrical Fault Conditions

A Dissertation submitted in fulfillment of the requirements for the Degree of

MASTER OF ENGINEERING
in
Power Systems

Submitted by

Nagendra Singh
(Reg. No. 801341010)

Under the Guidance of
Dr. Prasenjit Basak
Assistant Professor, EIED

2015

Electrical and Instrumentation Engineering Department
Thapar University, Patiala
(Declared as Deemed-to-be-University u/s 3 of the UGC Act., 1956)
Post Bag No. 32, Patiala – 147004
Punjab (India)

DECLARATION

I hereby certify that the work which is presented in dissertation entitled, "Modeling of DFIG based wind turbine mitigating dynamic behavior under varying load and asymmetrical fault conditions", in partial fulfillment of the requirements for the award of the degree of Master of Engineering in Power Systems, submitted to Electrical & Instrumentation Engineering Department of Thapar University, Patiala is as authentic record of my own work carried under the supervision of Dr. Prasenjit Basak. It refers others researcher's work which are duly listed in the reference section. The matter contained in this dissertation has not been submitted, neither in part nor in full to any other degree to any other university or institute except as reported in text and references.

Place: PATIALA
Date: 15/7/2015

(Nagendra Singh)
Roll No.: 801341010

It is certified that the above statement made by the student is correct to the best of my knowledge and belief.

Date: 15/7/15 .

(Dr. Prasenjit Basak)
Assistant Professor
Electrical & Instrumentation Engineering Department
Thapar University, Patiala

Countersigned by:

(Dr. Ravinder Agarwal)
Professor & Head
Electrical & Instrumentation Engineering Department
Thapar University, Patiala

(Dr. S. S. Bhatia)
Professor & Dean
(Academic Affairs)
Thapar University, Patiala

ACKNOWLEDGEMENT

With great pleasure and privilege, I wish to express my heartfelt sense of gratitude and indebtedness to Dr. Prasenjit Basak, Assitant Professor, EIED, Thapar University, Patiala for his patient guidance and support throughout this report. I found this guidance valuable and more importantly his supportive and motivating approach.

I am also thankful to Dr. Ravinder Agarwal, Professor & Head, EIED as well as Ms. Manbir Kaur, Associate Professor & PG Coordinator for the needed support and motivational approach. I also want to express my gratitude to Dr. Sanjay Kumar Jain, Associate Professor, for his valuable suggestion and constant encouragement all through the work.

I am also thankful to the faculty of EIED for extending their cooperation. I wish to thank my friends who devoted their valuable time and helped me in all possible ways towards successful completion of this work. I thank all those who have contributed directly or indirectly to this work.

Lastly, I would like to thank my parents for their years of unyielding love and encouragement. They have always wanted the best for me and admire their determination and sacrifice.

Nagendra Singh
(801341010)

TABLE OF CONTENTS

TABLE OF CONTENTS (Continued)

TABLE OF CONTENTS (Continued)

LIST OF TABLES

LIST OF FIGURES

LIST OF FIGURES (Continued)

LIST OF SYMBOLS

$\emptyset_{qdr}$	*dq*-axis rotor flux vector
$\emptyset_{qds}$	*dq*-axis stator flux vector
A	Swept area of the rotor
B	Friction coefficient
C_p	Power coefficient
D_{sh}	Mutual damping of the system
H_g	Inertia constant of generator
H_t	Turbine inertia constant
i_{qdL}	*dq*-axis current to coupling inductor
i_{qdLref}	Reference *dq*-axis current to coupling inductor
i_{qdr}	*dq*-axis rotor current
i_{qdrref}	Reference *dq*-axis current to rotor winding
i_{qds}	*dq*-axis stator current
$i_{qdsestim}$	Estimated value of *dq*-axis stator current
K_{sh}	Stiffness of the system
L	Coupling inductor
L_{lr}	Rotor leakage inductance
L_{ls}	Stator leakage inductance
L_m	Magnetizing inductance
L_r	Rotor inductance
L_s	Stator inductance
p	Pair of poles of DFIG
P_{air}	Power in the airflow
P_{meas}	Measured active power at grid terminal
P_s	Active power of the stator
P_t	Power captured by wind turbine
Q_{meas}	Measured reactive power at grid terminal
Q_{ref}	Reference reactive power at grid terminal

LIST OF SYMBOLS (Continued)

Q_s	Reactive power of the stator
R	Radius of the rotor blade
R	Coupling resistance
R_{cb}	Crowbar resistance
R_{ch}	DC chopper resistance
r_r	Rotor resistance
r_s	Stator resistance
T_e	Electromagnetic torque by DFIG
$T_{em\ cmd}$	Electromagnetic torque command
T_{sh}	Shaft torque
T_t	Aerodynamic torque of the wind turbine
U_{ctrl_grid}	Control voltage fed to GSC
U_{ctrl_rotor}	Control voltage fed to RSC
u_{qdr}	*dq*-axis rotor voltage
u_{qds}	*dq*-axis stator voltage
V_{dc}	DC-link voltage
V_{dcref}	Reference DC-link voltage
V_w	Upwind free wind speed
β	Blade pitch angle
θ_t	Shaft twist angle
λ	Tip speed ratio
ρ	Air density
ω_b	Base angular speed
ω_r	Angular speed of rotor of the generator
ω_{ref}	Reference angular speed of rotor of the generator
ω_s	Angular speed of stator flux
ω_t	Angular speed of wind turbine

LIST OF ABBREVIATIONS

BESS	Battery energy storage system
DFIG	Doubly-fed induction generator
DPC	Direct power control
FRC	Fully rated converter
GA	Genetic algorithm
GSC	Grid side converter
LVRT	Low voltage ride through
MPPT	Maximum-power point tracking
MSDBR	Modulated series dynamic braking resistor
PCC	Point of common coupling
PIR	Proportional integral resonant
PMSG	Permanent magnet synchronous generator
PWM	Pulse width modulation
RSC	Rotor side converter
SCIG	Squirrel-cage induction generator
SDR/SDBR	Series dynamic resistor/Series dynamic braking resistor
STATCOM	Static synchronous compensator
SVODPC	Stator oriented direct power control
TSR	Tip-speed ratio
VSC	Voltage source converter
WECS	Wind energy conversion system
WRSG	Wound-rotor synchronous generator
WT	Wind turbine

ABSTRACT

The integration of renewable energy resources, such as wind energy system, with utility grid is an important issue in the present power scenario. The study on performance of grid connected doubly fed induction generator (DFIG) based wind turbine (WT) system is relevant in this regard. DFIG has many advantages over other generators for variable speed application for harnessing wind energy through WT. In this work, a grid connected DFIG based WT is proposed considering voltage regulation and power loss as performance indicators of the system during varying load conditions at different locations. Ability of WT to stay connected to gird during grid fault is known as low voltage ride-through (LVRT) capability. Moreover, the studies on LVRT capability for DFIG based WT is a popular challenge for the researchers to propose a robust system considering variable load and severe fault conditions. Moreover, a comparative study is carried out between a crowbar and DC chopper protection schemes during severe asymmetrical fault condition resulting in satisfactory LVRT capability of proposed system. It is observed that the recovery period for DC chopper is increased as system reactive power requirement increased to settle DC-link voltage to its steady state value. Also it is found that the DC-link voltage is smoothened more in case of DC chopper protection compared to crowbar protection while DC chopper and crowbar resistances are set with same magnitude. The simulation results based on MATLAB-SimPowerSystems are explained.

CHAPTER-1

INTRODUCTION

1.1 Overview

Now a day it is well known fact that burning of fossil fuel affect the environment very significantly. Conventionally energy was produced by burning of fossil fuel. Burning of fossil fuel causes acid rain, global warming and many harmful organic compound in to the surrounding. But in case of renewable energy which includes solar, wind, geothermal and tidal energy, etc. the chances of pollution is less. Renewable energy has the benefits that it is clean, plentiful and inexpensive. Due to burning of fossil fuel 70 million metric tons of carbon emissions per year is produced in the atmosphere [1]. This carbon emission can be reduced by the use of renewable energy. Among the available renewable energy resources, wind energy is growing very fast [2]. Among all the available technologies for wind energy conversion system (WECS), the DFIG based WT is most accepted. This combination has advantages such as efficient power extraction due to variable speed operation and reduced rating of the converter [3].

Variable speed operation has more advantage as compared to fixed speed operation. There are three most widely used technology used in the industry for variable speed operation: (1) DFIG based WECSs having power converters of reduced capacity, (2) Geared or gearless SCIG based WECSs having power converters of full capacity, and (3) geared or gearless WRSG or PMSG based WECSs having power converters of full capacity. A WECS based on DFIG has many advantage such as [3]:

i. Efficiency of system is improved efficiency.
ii. Power Converter rating is reduced.
iii. Reduced losses and cost.
iv. Implementation of power factor correction unit is easy.
v. Variable speed operation and active and reactive power control can be achieved in all four quadrant.

Due to above advantages of variable speed operation, in case of DFIG based WT total energy output is 20%-30% higher. Thus capacity utilization factor is improved and cost per kWh energy is reduced.

In case of DFIG, stator circuit is directly supplied through network and the rotor circuit is supplied via back-to-back VSCs. This configuration controls rotor and stator power output supplied to network in case of variable speed operation [3]. Depending upon generator rotor speed, stator and rotor circuit both has capability of supplying power to network, in case of DFIG based WT. Active power flows from network to rotor circuit and RSC acts as a voltage source inverter and GSC acts as a rectifier for below synchronous speed. In case of above synchronous speed, RSC acts as a rectifier and GSC as voltage source inverter and thus real power flowing form rotor to RSC and then to network.

When a fault occurred at grid end, wind turbine should be connected to grid during voltage dip due to fault. Rotor current and DC bus voltage may exceed their threshold value so protection techniques are required to limit these values with in permissible limits.

1.2 Literature Review

T. Sun *et al.* (2004) [4], gave control strategy for DFIG based WT to recover voltage, in case of variable speed operation. Control approach suggests that generator rotor short circuited, and RSC is deactivated, while induction generator and GSC are connected with grid. Aerodynamic power is minimized by pitch control. After fault clearance and when voltage is recovered, RSC is again connected to system.

C. Zhan *et al.* (2006) [5], proposed additional series connected VSC to improve fault ride-through performance. This scheme is activated when DFIG experience a network fault at PCC.

Zhou Peng *et al.* (2007) [6], introduced stator oriented direct power control (SVODPC) and new control technique for the crowbar circuit in case of DFIG. This proposed method is capable of reducing the transient oscillations of the electromagnetic torque and fault current.

1.2 Literature Review

Ali H. Kasem *et al.* (2007) [7], suggested that both the converter RSC and GSC supply reactive power to the network during fault. A control mode named as transient control is provided to parallel converter for reactive power injection increment. In this crowbar resistance is connected across the rotor circuit during fault condition.

João P. A. Vieira *et al.* (2008) [8], presents a procedure based on genetic algorithm (GA) to obtain optimum PI controllers to the static converter to the rotor of DFIG. In this way a derivation of fitness function is done to express the time domain estimation of the DFIG with the objective to convince the DFIG continuous operation under grid fault.

Wei Zhang *et al.* (2008) [9], introduces different values of crowbar by-pass resistances and their impacts on the maximum fault currents and electromagnetic torque.

Olimpo Anaya-Lara *et al.* (2008) [10], suggested a resistor value that effects DFIG's rotor current, electrical torque and reactive power output. Two DFIG controllers, current control mode and flux magnitude and angle are chosen to optimize crowbar resistance.

Peng Zhou *et al.* (2008) [11], suggested a direct power control (DPC) method and a new crowbar protection method for DFIG. Transient oscillation in the electromagnetic torque and fault currents are suppressed by the use of DPC.

Dongdong Li *et al.* (2010) [12], implemented a technique in which crowbar is actuated to protect RSC and BESS is used to absorb unnecessary power stored in DC bus capacitor.

HAN Aoyang *et al.* (2010) [13], developed a combined current-voltage protection at PCC which could diminish the undesirable impact on protection produced by fault current characteristic of DFIG and certify that under fault ride through DFIG will operate, when network is subjected to a fault.

Chi Jin *et al.* (2010) [14], demonstrated a technique for grid fault condition, in which hysteresis control is used to reduce action time of crowbar circuit and unnecessary power is absorbed by BESS which is connected to DC bus.

1.2 Literature Review

K.E. Okedu *et al.* (2010) [15], compared two protective schemes, in the first case protection circuit is connected to DC bus and in the other case crowbar circuit is connected to rotor circuit of DFIG.

Wei Qiao *et al.* (2009) [16], demonstrated that the use of static synchronous compensator (STATCOM). STATCOM is used to improve transient voltage stability. Due to this DFIG based WT remain coupled to network during fault.

K.E. Okedu *et al.* (2011) [17], proposed and compared two methods using the synchronized control of the *dq*-axes measured currents of the RSC and series dynamic resistor (SDR) connected to the stator. Both schemes could limit rotor current of the DFIG within its minimal range during gird fault that can eliminate the need for a costly crowbar switch.

K. E. Okedu *et al.* (2012) [18], compared two schemes in which the DC-bus chopper-controlled braking resistor with additional control of RSC of the DFIG for the rotor circuit current and SDR is connected to stator of the DFIG.

Lihui Yang *et al.* (2012) [19], suggested that imbalance power is converted to kinetic energy of WT by RSC of DFIG. This can be achieved by increasing the rotor speed when a fault occurs at PCC.

Ma Hongwei *et al.* (2012) [20], proposed a method based on proportional integral resonant (PIR) controller for direct power control strategy of DFIG. A demagnetization method and a crowbar control strategy is used in coordination control scheme to improve LVRT capability.

S. Chandrasekaran *et al.* (2012) [21], demonstrated that to reduce the transient in current both during voltage drop and after fault clearance, a hysteresis current control method is proposed for crowbar protection and reactive power control.

Maoze Wang *et al.* (2012) [22], implemented a system consist of both DC hopper circuit and crowbar circuit to limit DC bus voltage and the rotor circuit current. Index is evaluated to check the effectiveness of the system.

Muhamad Zahim Sujod *et al.* (2013) [23], gave the scheme that initiates the rotor side converter to be at zero state switching, when transients arises in rotor circuit during grid fault then inner switching device are turned on and lower and upper switching devices are turned-off.

S. Abulanwar *et al.* (2013) [24], introduced a decoupled double synchronous reference frame (DDSRF) current controller is adopted for the design of GSC. Controller is used to counteract current oscillations during asymmetrical faults and reduces DC-link voltage ripple.

Po-Hsu Huang *et al.* (2015) [25], developed a method to increase fault ride-through of DFIG based WT. This scheme consist of a modulated series dynamic braking resistor (MSDBR) control. This proposed technique provide series voltage compensation and power is evacuated to mitigate the power imbalance during grid fault.

As electricity demand is increasing leaps and bounds day by day, we need some other energy resources to meet the demand. Wind energy is developing very fast among available resources of renewable energy. We need to connect these energy resources to the grid. During fault at the grid end WT must be connected to the grid. Some protection techniques are needed to increase the fault ride through of WECS.

1.3 Objective of the Work

As dispersion level of WTs into the grid increased, according to gird connection code requirement, WTs should be connected to the network during and after the fault, to maintain reliability of the system [19]. During grid faults, grid voltage decreases, causing sudden increase in rotor and stator circuit current and overvoltage in DC bus capacitor. In case of DFIG based WT power electronics converter are of reduced power rating so special attention to be paid towards the protection schemes.

Among available control strategy crowbar protection is most wildly used in industries. During fault, crowbar circuit, connected between RSC and rotor, is triggered and RSC is disconnected. Because of this rotor circuit experiences over current. Thus DFIG works as conventional induction machine. Due to this situation, induction machine absorbs reactive power from the faulty network [19].

Another method to control DC bus voltage and rotor current with in prescribed limit is to use DC Chopper circuit connected parallel with the DC bus capacitor. DC chopper is composed of power resistor in series with the power switch. In case of DC chopper, RSC is still connected to rotor of DFIG and DC chopper circuit will be activated.

1.4 Organization of the Dissertation

Presented work is divided in to six chapters. Chapter 1 contains the introduction to wind energy and the use of wind turbine in electrical power generation. It also includes overview of grid fault and protection techniques.

Chapter 2 discusses on the basic of wind energy generating system, WT component and wind turbine architecture (classification of wind turbine as per axis of rotation and as per speed).

Chapter 3 illustrates the modeling of major component of DFIG based wind turbine such as wind turbine, DFIG and drive train.

Chapter 4 discuss the validation of DFIG based WT model through study of basic control strategies pitch control, grid side converter control and rotor side converter control.

Chapter 5 is the result and discussion with a case study, in this chapter performance of DFIG under unsymmetrical fault with different types of protection techniques is applied in order to compare their effect on the DFIG behavior. DFIG is tested for different loading conditions, load is connected at different location and performance indices like voltage regulation and power loss is studied.

Chapter 6 is the conclusion of the thesis work and also it presents scopes for the future research work.

CHAPTER-2

WIND ENERGY GENERATING SYSTEM

Wind energy is fastest growing technology as compared to any other renewable energy resources. Following section deals with basic principle of wind power conversion, major component and architecture of WT.

2.1 Basic Theory of Wind Power Conversion

WT generate electricity by extracting mechanical energy of the air to drive the rotor of WT and this energy is converted to electrical energy by the electrical generator. Rotor of the WT turns a shaft which is connected to gearbox, and shaft transfer energy to gearbox. Gearbox is used to increase rotational speed which is appropriate to the generator, thus electricity is generated by converting rotational energy to electrical energy through magnetic field. The output power from the generator fed to a transformer, which is used to converts electricity for the utility.

WT works on the principle of extracting kinetic energy form the air that sweep across the blade area. The power in air (P_{air}) is as follows

$$P_{air}=\frac{1}{2}\rho A V_w^3 \tag{2.1}$$

Where

ρ = Density of air

A = Area swept by the WT rotor blade, m^2

V_w = Speed of the wind, m/sec

Availability of power in the air is reduced by a factor C_p (Power coefficient), which gives actual power available at the rotor of the WT (P_t):

$$C_p=\frac{P_t}{P_{air}} \tag{2.2}$$

Betz limit shows that the extreme value of C_p can never exceed 59.3%. This means power limited to 59.3% that can be extracted by the WT. In actuality, maximum value of C_p for WT is ranging from 25-45%.

There is one more term, Tip speed ratio (λ) that should be understood.

$$\lambda = \frac{\omega_r R}{V_w} \tag{2.3}$$

Where ω_r is the generator rotational speed, radius of the blade is R.

Tip-speed ratio, λ, and the power coefficient, C_p, are dimensionless quantities so they can describe performance of any dimension of the WT rotor.

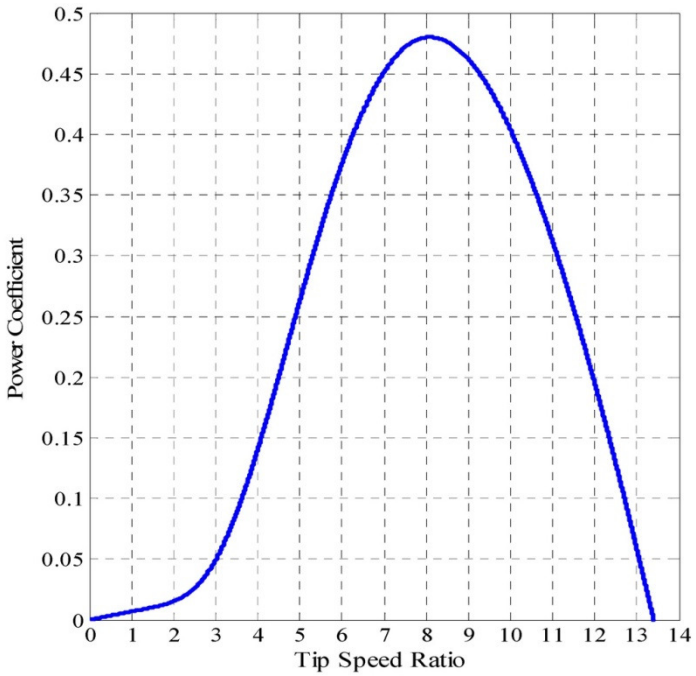

Fig. 2.1. Power coefficient vs. tip speed ratio curve [26]

Above Fig. 2.1 illustrates that the single tip speed ratio provide maximum value of C_p and for fixed velocity WT and this is achieved at single wind velocity. To operate the WT at variable speed change the value of C_p over wide range.

Power curve is used to describe power output of a WT at various wind speed. The power curve shows a graph between wind speed and the steady-state electrical power output as illustrated in Fig. 2.2.

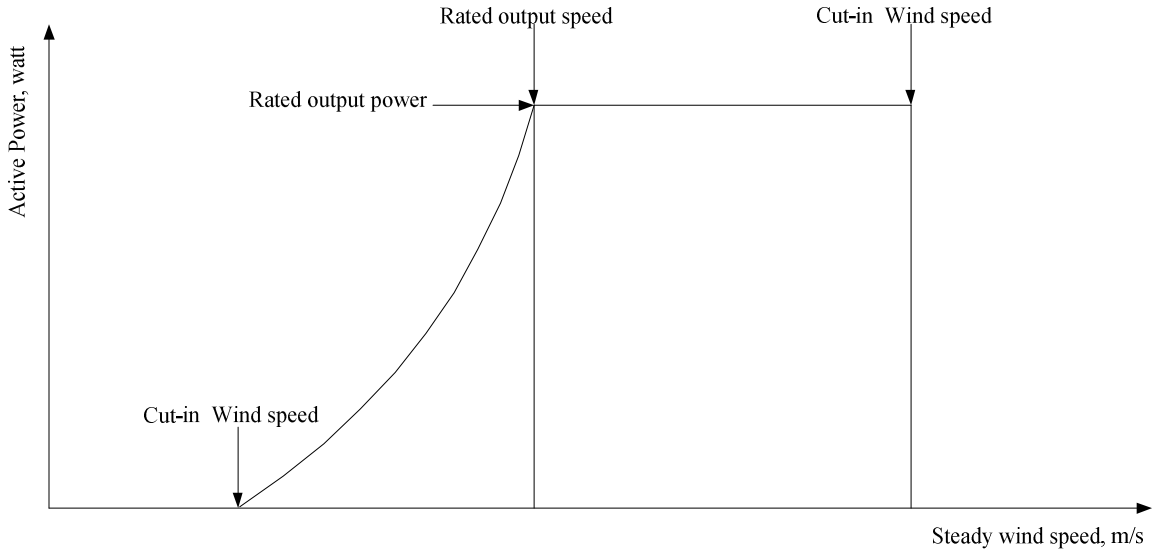

Fig. 2.2. Steady-state electrical output vs. wind speed [27]

Power curve has three main arguments on velocity scale:

- Cut-in wind speed – This is the lowest value of wind speed at which useful power is generated by the system.
- Rated wind speed – This is velocity of the wind at which rated power is achieved (rated power is defined as the maximum electrical power that can be generated by electrical generator).
- Cut-out wind speed – This is the maximum value of wind speed at which the turbine transport useful power.

2.2 Components of a Wind Turbine

Fig. 2.3 illustrates main component of WT are;

i. **Rotor:-**WT rotor blades are aero foil shaped. Wind make an impact on blades. Then rotor converts kinetic energy stored in the wind into mechanical energy by the use of shaft.

ii. **Gearbox:**-The Gearbox is used to step-up the rotational speed of the shaft to match with the generator.

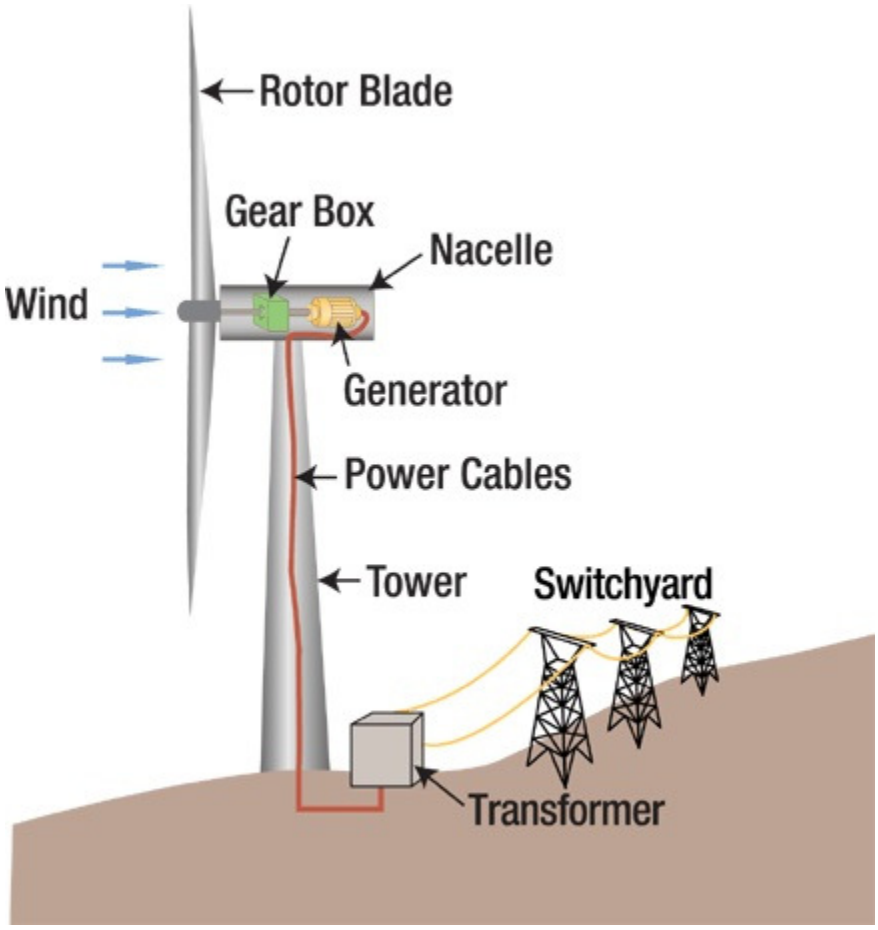

Fig. 2.3. Component of wind turbine [28]

iii. **Generator:**-Generator converts mechanical power to electrical energy.

iv. **Control and Protection system:**-Protection system does not allow the turbine to work under hazardous situation. This system includes the brake system which is operated by the signal when the wind speed is high, to stop the rotor from rotation.

v. **Tower:**-It is the tube that joints rotor of the WT to foundation. It improves the rotor height in air where stronger wind found.

vi. **Foundation:**-It supports the whole WT and it is fixed very properly onto the ground or roof of the house.

2.3 Wind Turbine Architecture

As per axis of rotation WTs are divided into two categories horizontal axis and vertical axis. As per wind speed there are two type of categories fixed speed and variable speed. The following section is mainly about above discussed categories.

2.3.1 Wind Turbine Classification as per Axis of Rotation

a) Horizontal axis wind turbine

In case of horizontal axis WT rotor axis blade is revolving parallel to ground and also parallel to wind flow. This type of configuration is the most common. There are two type of system one is upwind mode and other is down wind mode. In case of upwind mode rotor blade is upwind and in downwind mode wind blow past to tower before striking to the blade.

Most common horizontal axis WT mills are aero-turbine mills, having an efficiency of 35% and farm mills having an efficiency of 15%. Horizontal axis WT is shown in Fig. 2.4.

b) Vertical Axis Wind Turbine

A vertical axis WT has its rotor axis blade rotating perpendicular to the ground and need not to be oriented in the wind direction. Because horizontal axis wind turbine has vertical shaft, generator and transmission system can be mounted on the ground to facilitate easy maintenance, low cost, light weight of the tower.

As compared to horizontal axis WT there are very few vertical axis WT because at higher elevations and at strong wind speed they do not provide any advantage.

Darrieus is the simple vertical axis design. It has curved blade and having an efficiency of 35%. Other design is Giromill having straight blade and efficiency of 35%. Third one is Savonius, having scoops for catching the wind and the efficiency of 30%. Vertical axis WT is portrayed in Fig. 2.4.

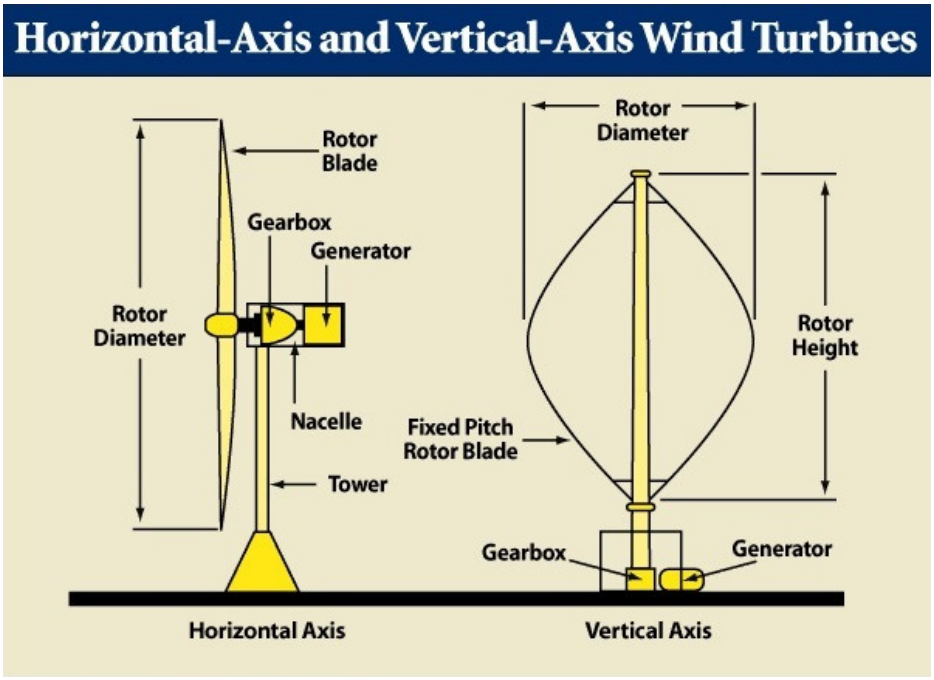

Fig. 2.4. Horizontal-Axis and Vertical-Axis wind turbines [29]

2.3.2 Wind Turbine Classification as per Speed

a) Fixed-Speed Wind Turbines

These turbines are electrically simple in design. Its rotor driving a low-speed shaft then it drives a gearbox. Output of gearbox is given to high speed shaft and then to generator. Wind stream apply torque on the low speed shaft so they are considered as large fan drives.

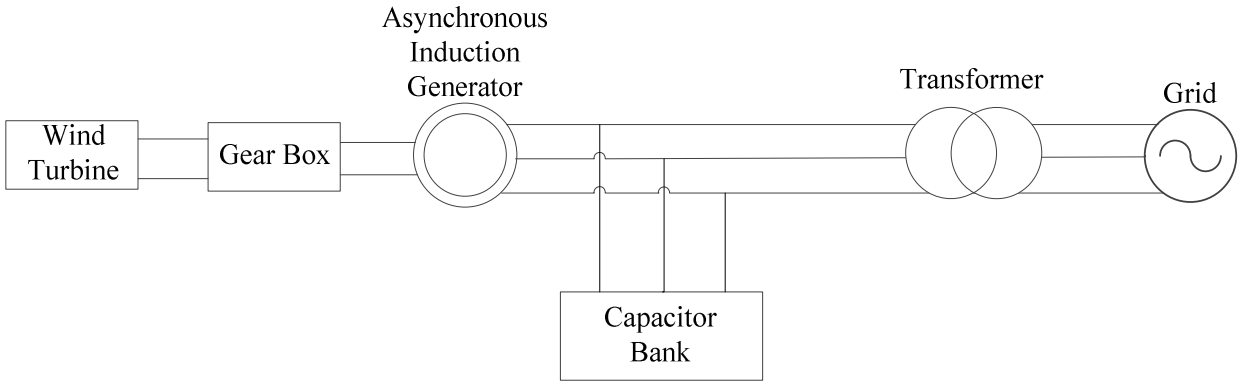

Fig. 2.5. Schematic of a fixed-speed wind turbine [27]

It consist of squirrel-cage induction generator connected to via a transformer. Although variation of slip is 1%, they are referred as fixed speed WT. Power factor correction unit is provided at each location of WT because Squirrel-cage induction machines are absorber of reactive power.

b) Variable-Speed Wind Turbines

As Size of WTs increased day-by-day, technology has moved to variable speed from fixed speed. The main reason behind this is to fulfill grid code connection requirement and also mechanical loads are reduced due to variable speed. There are two types of variable-speed WT, which are as follows:

1) Doubly fed induction generator (DFIG) wind turbine
2) Fully rated converter wind turbine

1) Doubly Fed Induction Generator (DFIG) Wind Turbine

As name suggests "Doubly fed" means stator of the induction machine is supplied via grid and rotor is supplied with back-to-back VSCs. Wound-rotor induction generator, having slip rings, is used in DFIG based WT. Power is supplied to machine and taken out of the rotor via slip rings. By supplying a controlled voltage to rotor at slip frequency variable speed operation of the system is achieved. The VSCs decouples electrical frequency of the network from mechanical frequency of the rotor, thus WT with variable-speed achieved.

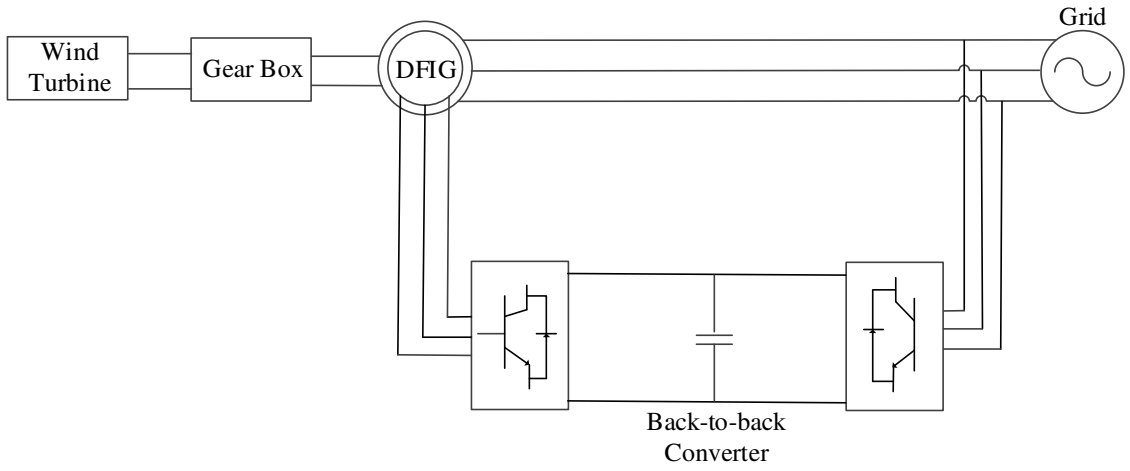

Fig. 2.6. Typical configuration of a DFIG wind turbine [27]

In case of DFIG system power is supplied to grid through stator and rotor, in some cases rotor absorb power. Speed of generator is responsible for this type of power flow. If generator is operating above synchronous speed, termed as super-synchronous mode, power is supplied to the network by rotor through converter, and if generator operates below synchronous speed, termed as sub-synchronous mode, rotor is supplied by grid.

2) Fully Rated Converter (FRC) Wind Turbine

Gearbox may or may not be employed in fully rated converter WT and wide range of electrical generators like PMSG or WRSG can be used. It is called as FRC WT because whole power goes through the power converter. Power grid cannot access dynamic operation of electrical generator. Grid frequency changes when wind speed changes but there is no change in grid frequency. Thus WT can attain variable speed operation.

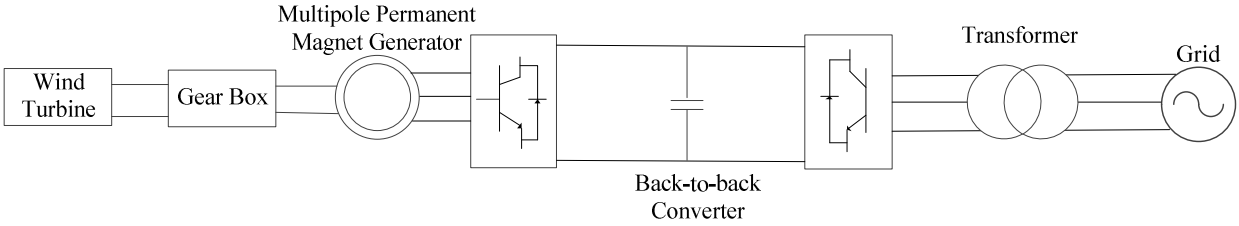

Fig. 2.7. Configuration of a FRC-connected wind turbine [27]

Power converters can be linked by many means. Two VSCs, termed as generator-side converter and network-side converter, are arranged in such a way generator action is controlled and power flows to grid. Network-side converter controls the DC-link voltage and generator-side converter is used to control the torque applied to generator. Control idea can be reversed. Reactive power can be absorbed and generated by each converter independently.

CHAPTER-3

MODELING OF DFIG BASED WIND TURBINE

The diagram of DFIG based WT coupled to grid is shown in Fig. 3.1. The DFIG based WT system consist of WT, drive train, DFIG, back-to-back voltage source converter (VSC), and control system. This system is connected to grid through transformer. Control system consists of two control levels. First one is WT control and the other is DFIG control. In case of WT control, pitch angle is used to control output mechanical power of the WT. WT control also generates reference speed for generator at given speed of the wind and power-speed characteristic. For DFIG control, that consist of GSC and RSC controllers. These are used to control active and reactive power of DFIG through vector control technique.

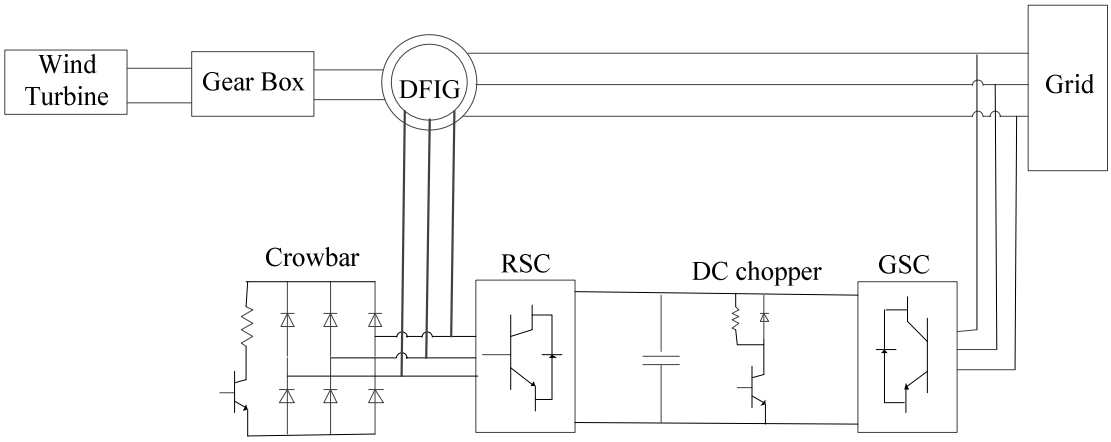

Fig. 3.1. Schematic diagram of the DFIG WT system [30]

3.1 Wind Turbine Model

The WT is described by the power it generates. Power through WT is function of the wind velocity, air density, radius of the turbine and power coefficient for the turbine. Blades of the turbine play an significant role in energy capture. If the radius of WT rotor is large, then it will capture large amount of energy from the wind [3].

$$P_t = \frac{1}{2}\rho A V_w^3 C_p(\lambda,\beta) \tag{3.1}$$

Where ρ is density of air (kg/m^3), A is the area swept via rotor blades (m^2), V_w is the wind speed (m/s) and power coefficient is C_p, and

$$C_p(\lambda,\beta)=0.5176\left(\frac{116}{\lambda_i}-0.4\beta-5\right)e^{-\frac{21}{\lambda_i}}+0.0068\lambda \tag{3.2}$$

$$\lambda_i=\frac{1}{\frac{1}{(\lambda+0.08\beta)}-\frac{0.035}{(\beta^3+1)}} \tag{3.3}$$

The power coefficient C_p is the ratio of power output from WT to the existing power in the air. C_p is defined as maximum power the WT can captivate from the existing wind power at a given wind velocity. It can be represented as a function of the tip speed ratio and blade pitch angle. The pitch angle of the blade is controlled by pitch controller and TSR is presented in (2.3).

In general, the aerodynamic torque produced by the wind turbine (T_t) can be expressed as [3]

$$T_t=\frac{1}{2}\frac{\rho\pi R^3 V_w^2 C_p(\lambda,\beta)}{\lambda} \tag{3.4}$$

Thus by controlling rotational speed of the generator, TSR can be controlled. For single wind speed, there is one rotational speed of generator that provides maximum value of C_p at a given blade pitch angle. This is the basic theory behind maximum-power point tracking (MPPT) and WT are designed by taking care of this approach [3].

3.2 Mathematical Model of DFIG

A mathematical model is the best way to understand the behavior of complex system. odel is used to understand different operating condition and for the analysis of control strategies. Mathematical model of DFIG is derived in direct and quadrature axes (*dq* axes) quantities. This *dq* axes quantities are rotating in synchronism with the stator flux vector. An equivalent circuit of DFIG in the synchronous rotating reference frame is illustrated in Fig. 3.2 [3].

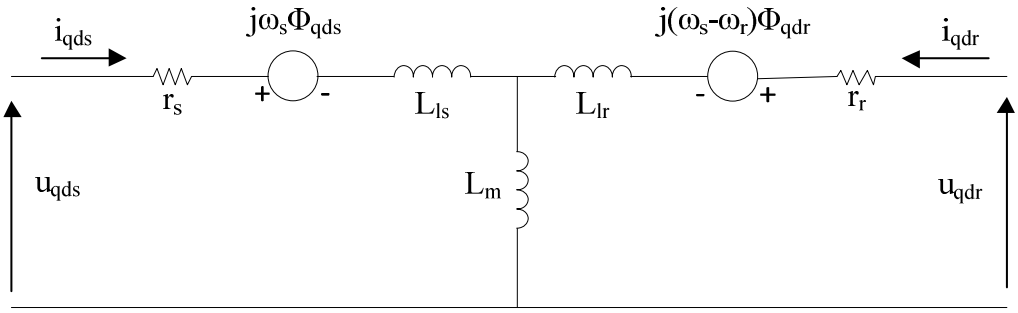

Fig. 3.2. Complex synchronous equivalent of a DFIG [3]

$$u_{qds}=r_s i_{qds}+j\omega_s \emptyset_{qds}+\frac{d\emptyset_{qds}}{dt} \tag{3.5}$$

$$u_{qdr}=r_r i_{qdr}+j(\omega_s-\omega_r)\emptyset_{qdr}+\frac{d\emptyset_{qdr}}{dt} \tag{3.6}$$

$$\emptyset_{qds}=L_s i_{qds}+L_m i_{qdr} \tag{3.7}$$

$$\emptyset_{qdr}=L_r i_{qdr}+L_m i_{qds} \tag{3.8}$$

$$T_e=\frac{3}{2}\frac{p}{2}\mathrm{Re}[j\emptyset_{qds}.\overline{i_{qds}}]$$

$$=\frac{3}{2}\frac{p}{2}\mathrm{Re}[j\emptyset_{qdr}.\overline{i_{qdr}}] \tag{3.9}$$

where $\overline{i_{qds}}$ and $\overline{i_{qdr}}$ are stator current and rotor current space vector in the complex conjugate form, u_{qds} and u_{qdr} are complex conjugate of stator voltage and rotor voltage vector and Φ_{qds} and Φ_{qdr} are complex conjugate of stator flux and rotor flux vector. Stator and rotor inductances are given as

$$L_s=L_{ls}+L_m \tag{3.10}$$

$$L_r=L_{lr}+L_m \tag{3.11}$$

The complex torque (T_e) equation of (3.9) can be resolute in the reference *dq* axes leading to

$$T_e=\frac{3}{2}\frac{p}{2}\left(\emptyset_{ds}i_{qs}-\emptyset_{qs}i_{ds}\right)=\frac{3}{2}\frac{p}{2}\left(\emptyset_{dr}i_{qr}-\emptyset_{qr}i_{dr}\right) \tag{3.12}$$

The active and reactive powers on the stator side are given as

$$P_s=\frac{3}{2}Re[u_{qds}.\overline{i_{qds}}=\frac{3}{2}[v_{qs}i_{qs}+v_{ds}i_{ds}]$$
$$Q_s=\frac{3}{2}Im[u_{qds}.\overline{i_{qds}}=\frac{3}{2}[v_{qs}i_{ds}-v_{ds}i_{qs}] \quad (3.13)$$

Considering that

$$\overline{i_{qds}}=\frac{1}{L_s}\overline{\emptyset_{qds}}-\frac{L_m}{L_s}\overline{i_{qdr}} \quad (3.14)$$

The modified active and reactive power equations are as follows

$$P_s=\frac{3}{2}\left\{\frac{1}{L_s}\left(u_{qs}\emptyset_{qs}-u_{ds}\emptyset_{ds}\right)-\frac{L_m}{L_s}\left(u_{qs}i_{qr}+u_{ds}i_{dr}\right)\right\} \quad (3.15)$$
$$Q_s=\frac{3}{2}\left\{\frac{1}{L_s}\left(u_{qs}\emptyset_{qs}+u_{ds}\emptyset_{ds}\right)-\frac{L_m}{L_s}\left(u_{qs}i_{dr}-u_{ds}i_{qr}\right)\right\} \quad (3.16)$$

Thus, stator currents magnitude controls the active and reactive powers of the stator. These currents depend on the rotor currents. By controlling the rotor currents (i_{qr} and i_{dr}) in WECS the active and reactive powers can be controlled.

3.3 Drive Train Model

To better understand the dynamic stability of DFIG based WT, the two mass model of the drive train is very important. As the WT shaft is much more softer than the steam turbine shaft in conventional power plants [19]. Fig. 3.3 illustrates the drive train modeling considering two mass system of WT.

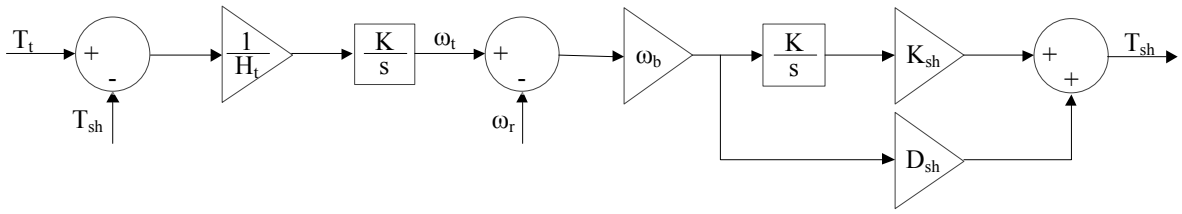

Fig. 3.3. Schematic diagram of Drive train [31]

Equations representing two-mass model of the drive train is given as follows

$$\frac{d\omega_r}{dt}=\frac{1}{2H_g}(T_{sh}-T_e-B\omega_r) \tag{3.17}$$

$$\frac{d\theta_t}{dt}=\omega_b(\omega_t-\omega_r) \tag{3.18}$$

$$\frac{d\omega_t}{dt}=\frac{1}{H_t}(T_t-T_{sh}) \tag{3.19}$$

Where ω_t is the wind turbine speed. H_t and H_g are the inertia constant of turbine and generator, respectively. B is the generator friction coefficient, θ_t is the twist angle of the shaft, given in radian (rad.). Shaft torque T_{sh}, and mechanical torque T_t input of the WT are given as:

$$T_{sh}=K_{sh}\theta_t+D_{sh}\omega_b(\omega_t-\omega_r) \tag{3.20}$$

$$T_t=\frac{1}{2}\frac{\rho\pi R^2C_p(\lambda,\beta)V_w^3}{\omega_t} \tag{3.21}$$

CHAPTER-4

CONTROL OF DFIG

Main purpose of DFIG controller is to control the bidirectional power flow, which can be achieved by two converters with intermediate DC-link capacitor, between stator and rotor circuit. There are three basic control for the DFIG based WT.

1) For very strong wind speed, pitch control is used to control input power till the wind speed shutdown limit is reached. This is done to optimize the power extraction from the wind in case of very high wind speed.
2) By controlling rotor current of DFIG through RSC, real and reactive power produced by DFIG can be independently controlled
3) GSC is used to control the DC bus voltage and to set unity power factor operation.

For the decoupled control of rotor excitation current and torque of DFIG, vector control techniques are used. Through this technique active and reactive power supplied to grid can be independently controlled. By controlling the active power generator rotor speed can be controlled thus speed of the rotor of the WT.

Control strategies for pitch, GSC and RSC are discussed in the following section.

4.1 Pitch Control

Pitch angle of the blade is controlled to optimize the power extraction of the WT. This also helps to avoid power production in very strong wind [19]. The pitch angle control is illustrated in Fig. 4.1.

When measured generated speed, ω_r exceeds reference speed, ω_{ref} from the tracking characteristic corresponding to actual power P_{meas} then pitch angle control is activated and pitch angle is changed such that power from the limited to rated value.

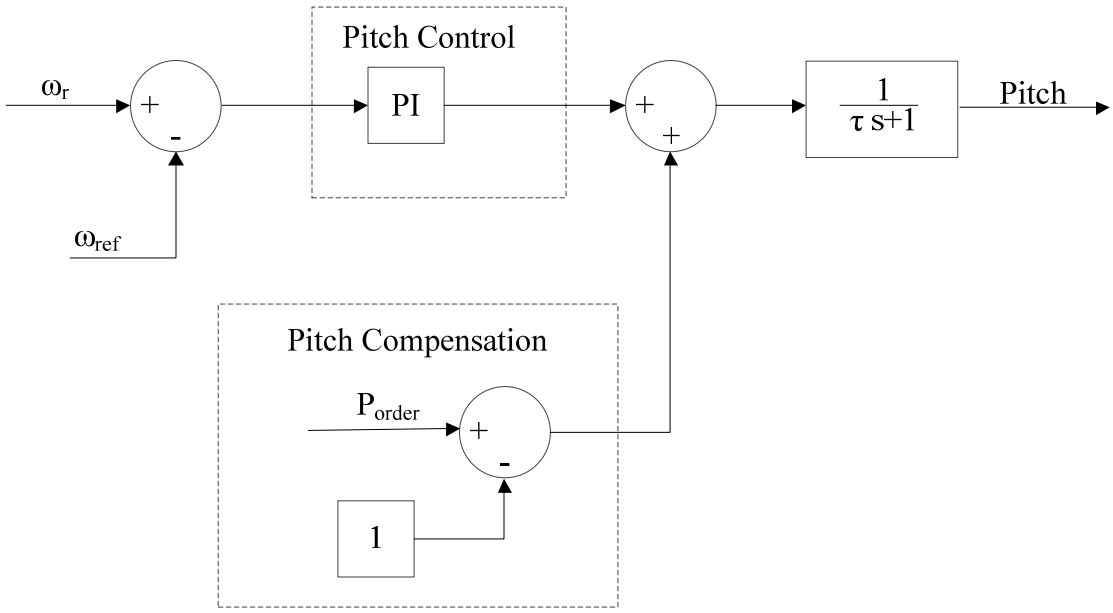

Fig. 4.1. Schematic diagram of pitch control [31]

4.2 Grid Side Converter Control

Purpose of Grid-side converter (GSC) is to control DC bus voltage and to maintain grid converter reactive current to zero. Fig. 4.2 shows the system that is used to control DC bus voltage and gird converter reactive current.

Control system consist of DC bus voltage regulator, in which actual value of DC bus voltage (V_{dc}) is compared with the reference value (V_{dcref}). By the use of PI controller, error is reduced to zero. Output from DC bus voltage controller is the reference *d* axes current (i_{dLref}). Actual value of *d* axes current (i_{dL}) is compared with the (i_{dLref}) and error is reduced to zero by the use of current regulator. Reference *q* axes current (i_{qLref}) is set to zero. A comparison is done between actual *q* axes current (i_{qL}) and with the reference value and error so produced is reduced to zero through current controller. Output from the current regulator, *dq*-axis voltage u^*_{dg} and u^*_{qg} which is transformed into ABC. For PWM generation of the GSC, these control voltages (U_{ctrl_grid}) are used.

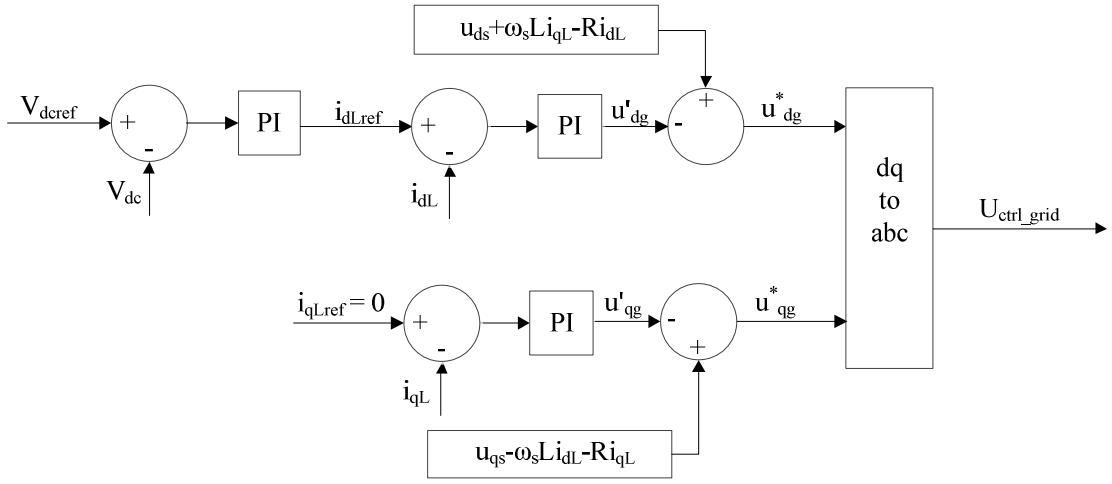

Fig. 4.2. Control system for grid-side converter [31]

4.3 Rotor Side Converter Control

RSC controls the reactive power at the network and generator speed. Generator speed is regulated to track pre-defined power-speed characteristic. This characteristic is called as tracking characteristic. At grid terminal of DFIG actual power is measured Pmeas and speed corresponding to that speed is used as reference speed for the speed regulator. Speed regulator is illustrated in Fig. 4.3.

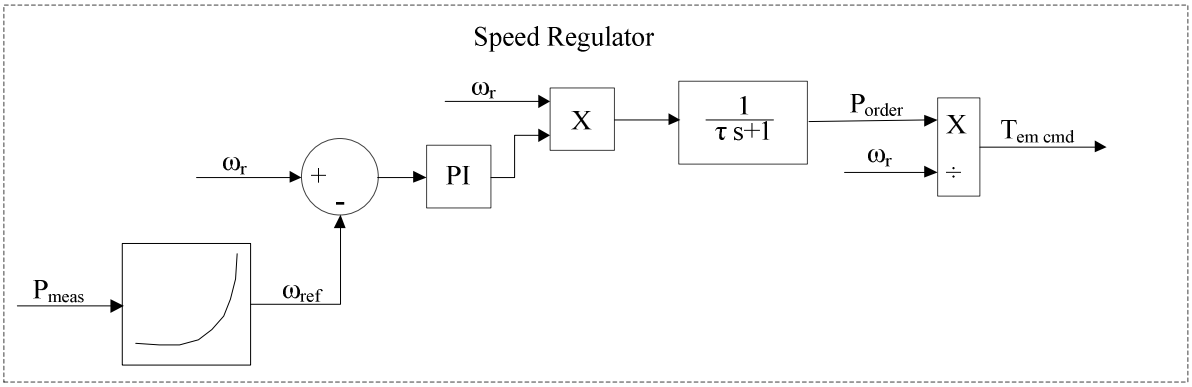

Fig. 4.3. Schematic diagram of speed regulator [31]

Electromagnetic torque ($T_{em\ cmd}$) that is generated by the generator which is output from the speed controller. Control of electromagnetic torque and reactive power is illustrated in Fig. 4.4. The *d* axes of rotating reference frame is aligned with the positive-sequence of stator

voltage. This is done by using the phase-locked loop. $T_{em\ cmd}$ is divided by magnitude of flux of the generator to obtain reference rotor current (i_{drref}) that must be supplied by RSC.

The actual value of d-axis rotor current (i_{dr}) is compared with (i_{drref}). The error is reduced to zero by the use of current controller. Output from this current controller is *d* axis voltage (u^*_{dr}) that must be generated by RSC.

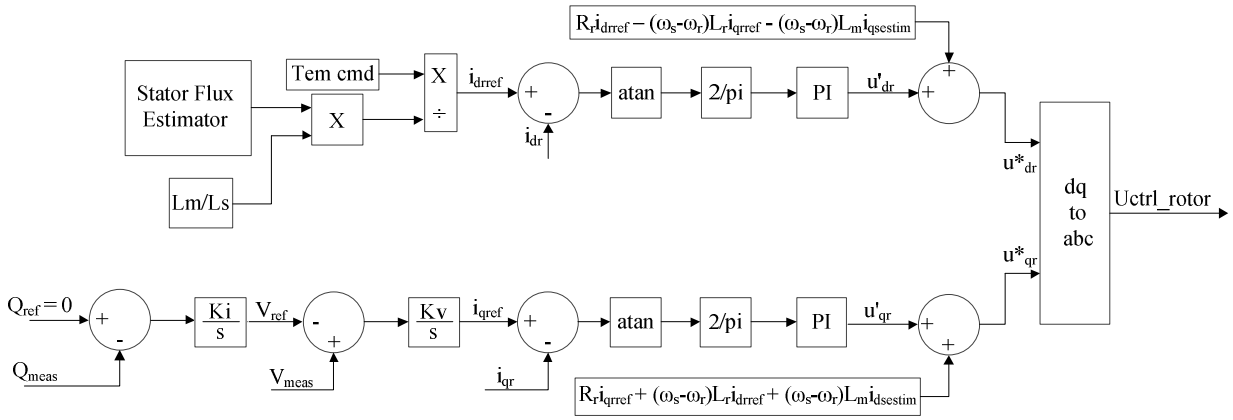

Fig. 4.4. Control system for rotor-side converter [31]

As for the reactive power is concerned it is measured (Q_{meas}) at grid terminal of DFIG and compared with the reference value (Q_{ref}), which is taken as zero for unity power factor operation. Error is reduced to zero by the integral regulator, known as var regulator.

Output from var controller is the voltage reference (V_{ref}) at the network terminal of DFIG. The real value of voltage (V_{meas}) is compared with the reference voltage (V_{ref}). The error from the voltage controller is reduced to zero by an integral controller. Output from this voltage controller is q-axis rotor current (i_{qrref}) that should be supplied to rotor by RSC. Actual value of q-axis rotor current (i_{qr}) is compared with reference value of *q* axes current (i_{qrref}). The error is reduced to zero by the use of current controller same as used for electromagnetic torque.

Output of the current regulator is q-axis voltage (u^*_{qr}) that must be generated by RSC. Output from the current regulator, *dq*-axes voltage which is transformed into ABC. For the PWM

generation of the RSC, these control voltages are used. Estimated values of stator *dq*-axes stator currents $i_{dsestim}$ and $i_{qsestim}$ can be calculated as

$$i_{dsestim}=\left[u_{ds}-\omega_s^2\frac{L_mL_s}{R_s}i_{drref}+\omega_sL_mi_{qrref}\right]\frac{R_s}{\omega_s^2L_s^2+R_s^2} \tag{4.1}$$

$$i_{qsestim}=-[i_{dsestim}]\frac{\omega_sL_s}{R_s}-\frac{\omega_sL_m}{R_s}i_{drref} \tag{4.2}$$

CHAPTER-5

LOW VOLTAGE RIDE THROUGH STRATEGY

Due to fault at the gird end there is a dip in the voltage to a low level, thus causing the electrical power output to greatly reduce. Stator voltage decreased due to dip in the grid voltage. Stator and rotor are electromagnetically coupled circuit so decrease in the voltage cause surge current in the rotor circuit. Because of increase in rotor circuit current, electromagnetic torque increases to unexpected level causing mechanical force to impairment of whole system.

Ability of WT to remain connected to the system is called as LVRT capability. To fulfill LVRT capability of DFIG based WT may enforce design challenges, specially:

i. Protection of the converter circuit against the overvoltage and overcurrent and maintain DC bus voltage within limits.
ii. During network instability, lessening of stress on mechanical shaft.
iii. To eliminate or reduce absorption of reactive current from the gird during and after recovery from the fault.

Among available control strategies crowbar protection and DC chopper protection is commonly used. Above mentioned techniques are in detail in the following sections.

5.1 Crowbar Protection Scheme

Crowbar is used to protect the converter because of reduced cost and easy design. The crowbar triggers when the rotor current or DC bus voltage surpasses the limits. DFIG acts as fixed speed induction generator, when crowbar is triggered. In this situation rotor resistance is increased. Because of addition of rotor resistance speed shifted to a position at which break down torque occurs at low slip (higher speed). This diminishes the reactive power absorption [32].

Rotor circuit fault current exceeds crowbar current limit during fault. By the use of high energy dissipation resistor, crowbar short-circuits the rotor terminal. Due to this fault current is

reduced and as a consequence RSC terminals are open. Crowbar by-passes the resistor and reconnection of RSC take place when the rotor fault current lessens to a tolerable limit.

A crowbar circuit is placed in between RSC and rotor of DFIG. Crowbar circuit provides a detour for high transient rotor fault current which appear in the system due to voltage dip in the grid. When crowbar circuit is activated during fault at the grid end, RSC will be blocked. As illustrated in Fig. 5.1, crowbar circuit is made up of three-phase uncontrolled bridge rectifier and a detour resistor.

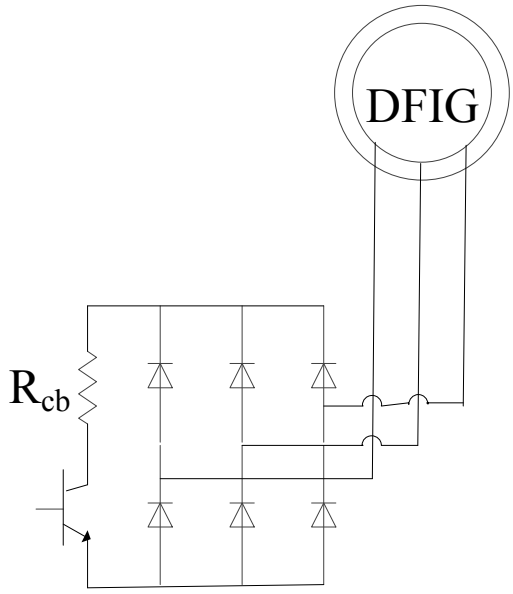

Fig. 5.1. Schematic diagram of crowbar protection circuit [32]

A passive crowbar is no longer in use. An active crowbar used to protect DFIG against overvoltage and to limit rotor current with in permissible value during grid faults.

5.2 DC Chopper Protection Scheme

The DC chopper composed of power resistor which is connected in parallel to DC capacitor through a power switch. The switch will be turn off if the DC bus voltage is within predefined limits. When fault occurs at the grid, grid voltage drops. DC-link capacitor experiences overvoltage during grid voltage dip. To protect capacitor from overvoltage DC chopper is connected in parallel with capacitor [33].

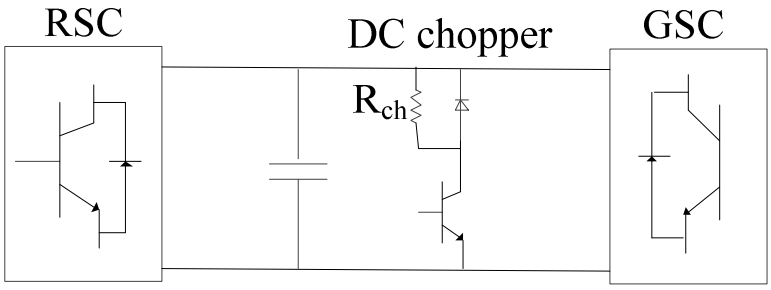

Fig. 5.2. Schematic diagram of DC chopper protection circuit [32]

When DC-link voltage exceeds the threshold value DC chopper will be on and RSC remain coupled to the rotor of DFIG. When DC-link voltage restored to predefined value, DC chopper will turned off. Fig. 5.2 illustrates the proposed DC chopper circuit.

CHAPTER-6

RESULT AND DISCUSSION: A CASE STUDY

To investigate the performance of DFIG based WT system, a sample power system is modeled using MATLAB-SimPowerSystem software as shown in Fig. 6.1.

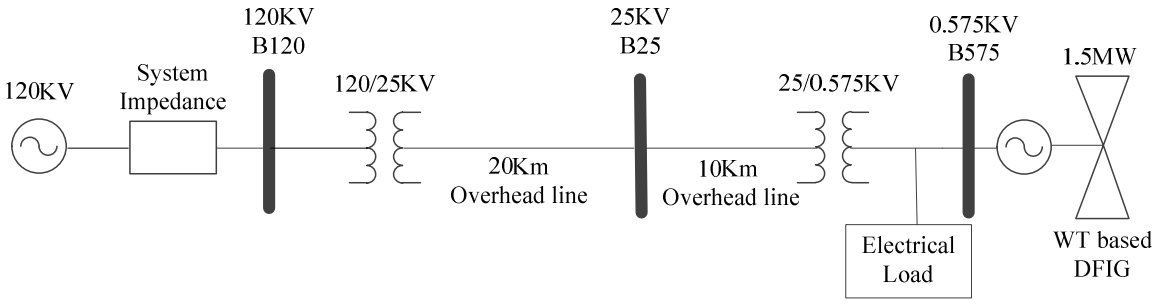

Fig. 6.1. System configuration

A WT connected to DFIG having capacity of 1.5 MW is considered for the study. Pitch controlled WT is used for the study. WT connected to 25 kV bus via a 575V/25 kV, 2 MVA transformer. This DFIG based WT connected to grid of 120 kV via a 120 kV/25 kV, 47 MVA transformer. Key parameters are shown in table 6.1 [31], [34] for the DFIG. To evaluate the effectiveness of the different loading condition and LVRT protection techniques simulation have been performed using MATLAB-SimPowerSystems. A fixed speed of 15m/s is used for entire simulation.

Based on the above mentioned model the following studies are carried out to validate the performance of the proposed DFIG based WT system.

(i) Study of system response for varying loading conditions and at different positions along the transmission line

(ii) Protection techniques during LVRT

  (a) Without any protection

  (b) With crowbar protection

  (c) With DC chopper protection

Table 6.1. Parameters of the DFIG

Parameters	DFIG
Rated capacity of machine (MW)	1.5
Power factor	0.9
Rated voltage (V)	575
Rated frequency (Hz)	60
Stator leakage impedance(L_{ls}) (p.u.)	0.18
Rotor leakage impedance(L_{lr}) (p.u.)	0.16
Magnetizing inductance(L_m) (p.u.)	2.9
Number of pole pairs	3
Nominal DC bus voltage (V)	1150
DC bus capacitor (F)	0.01
Rotor speed (p.u.)	1.2

6.1 System Response for Varying Loading Conditions and at Different Positions

DIFG based WT is subjected to different loading conditions and at different locations along the transmission line, to study the performance indices of the system like voltage regulation and power loss. Firstly load is connected at the DFIG and then at the grid.

6.1.1 Load Connected Near DFIG

Load is connected at bus B575 and load is increased from 25% of rated capacity of the DFIG to 200% and load power factor is taken 0.9 as constant.

Table 6.2 illustrates that if a load is below rated capacity of the DFIG then active power flows from DFIG to grid and to the load. In 3rd row of table 6.2 real power from the WT is 1.314 MW which is supplied to load of 1.074 MW (75% of rated capacity of the DFIG) and rest of the real power supplied to grid (0.236 MW) and transmission line losses.

If the load is at its rated capacity or more the active power is shared by the DFIG and grid. In the 6th row of table 6.2 the real power demand of the electrical load 2.014 MW (150% of rated capacity of the DFIG) which is to be supplied by WT (1.317 MW) and grid (0.706 MW).

Table 6.2. Active and reactive power sharing between grid and DFIG when electrical load is at bus B575

Sr. No.	% of rated load of DFIG	Electrical load			B25		B575		Load	
		Apparent Power	Real Power	Reactive Power						
		S (MVA)	P (MW)	Q (MVAR)	P (MW)	Q (MVAR)	P (MW)	Q (MVAR)	P (MW)	Q (MVAR)
1	25	0.417	0.375	0.182	-0.929	0.183	1.308	-0.001	0.373	0.181
2	50	0.833	0.750	0.363	-0.555	0.344	1.290	-0.003	0.730	0.353
3	75	1.250	1.125	0.545	-0.236	0.506	1.314	-0.002	1.074	0.520
4	100	1.667	1.500	0.726	0.081	0.674	1.325	-0.006	1.401	0.678
5	125	2.083	1.875	0.908	0.405	0.840	1.315	-0.007	1.714	0.830
6	150	2.500	2.250	1.090	0.706	1.002	1.317	-0.001	2.014	0.976
7	175	2.917	2.625	1.271	0.975	1.169	1.337	-0.002	2.302	1.115
8	200	3.333	3.000	1.453	1.241	1.338	1.344	-0.004	2.572	1.246

As load is increased from 25% to 200% of rated capacity of the DFIG, power loss is decreased for the value of 125% and it is again increased thereafter as shown in Fig. 6.2. Voltage regulation as presented in Fig. 6.3, shows satisfactorily result.

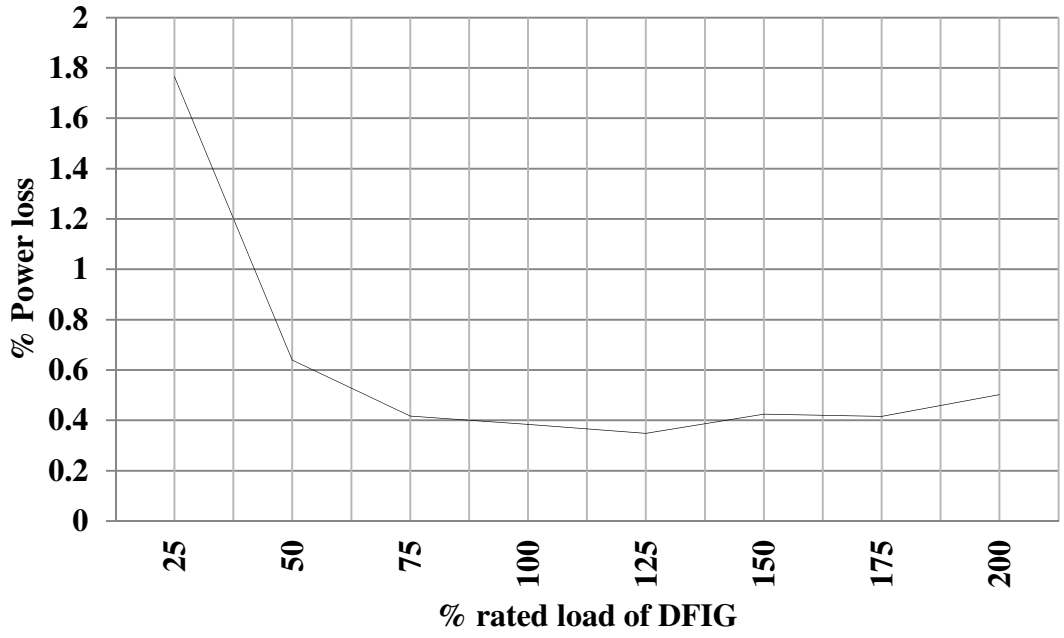

Fig. 6.2. Power loss (%) vs. Rated load of DFIG (%), load at bus B575

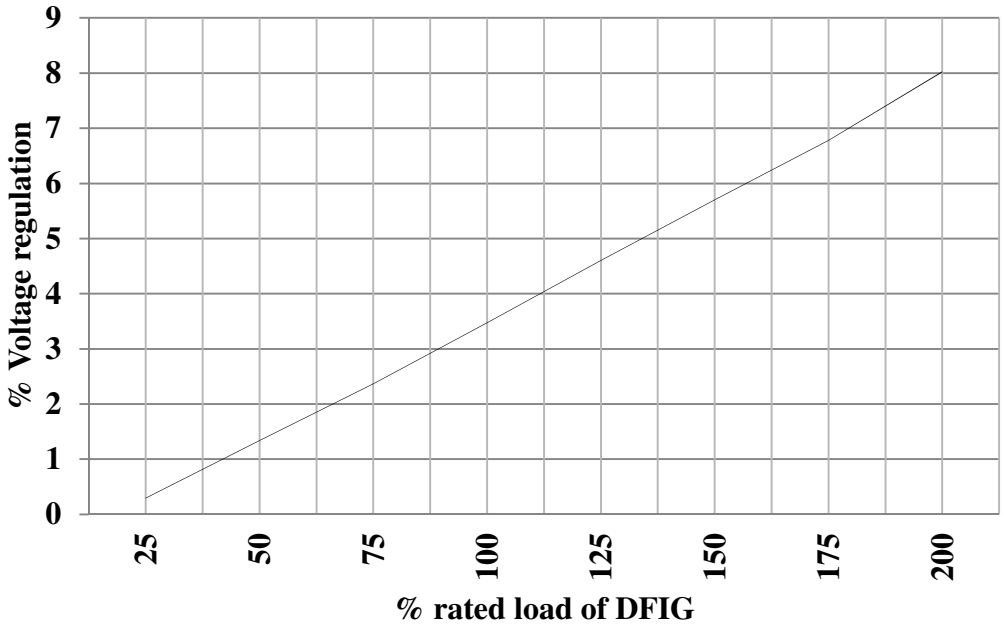

Fig. 6.3. Voltage regulation (%) vs. Rated load of DFIG (%), load at bus B575

6.1.2 Load Connected Near GRID

Load is connected at bus B25 and load is increased from 25% of rated capacity of the DFIG to 200% and load power factor is taken 0.9 as constant same as above case.

Table 6.3 depicts that DFIG will supply real power to load and grid if load is below rated capacity of the DFIG. In 2nd row of table 6.3 real power requirement of the load is 0.744 MW (50% of rated capacity of the DFIG) which is supplied by the WT (1.29 MW) and rest of the real power is supplied to grid (0.170 MW) and the transmission line.

For rated or more than rated capacity of the load, DFIG and grid both will share the active power and the transmission line losses. In the 7th row of table 6.3, WT (1.314 MW) and grid (1.188 MW) will feed real power demand of the load (2.493 MW) and transmission line losses.

6.1 System Response for Varying Loading Conditions and at Different Positions

Table 6.3. Active and reactive power sharing between grid and DFIG when electrical load is at bus B25

Sr. No.	% of rated load of DFIG	Electrical load			B25		B575		Load	
		Apparent Power	Real Power	Reactive Power						
		S (MVA)	P (MW)	Q (MVAR)	P (MW)	Q (MVAR)	P (MW)	Q (MVAR)	P (MW)	Q (MVAR)
1	25	0.417	0.375	0.182	-0.936	0.220	1.320	-0.010	0.375	0.182
2	50	0.833	0.750	0.363	-0.537	0.389	1.290	-0.003	0.744	0.360
3	75	1.250	1.125	0.545	-0.170	0.561	1.284	0.001	1.106	0.536
4	100	1.667	1.500	0.726	0.187	0.737	1.283	-0.003	1.462	0.708
5	125	2.083	1.875	0.908	0.525	0.905	1.296	0.001	1.812	0.878
6	150	2.500	2.250	1.090	0.856	1.073	1.308	0.001	2.156	1.044
7	175	2.917	2.625	1.271	1.188	1.238	1.314	0.000	2.493	1.207
8	200	3.333	3.000	1.453	1.553	1.396	1.280	0.001	2.824	1.368

As load is increased from 25% to 200% of rated capacity of the DFIG, power loss is decreased as load is increased as shown in Fig. 6.4. Voltage regulation as presented in Fig. 6.5, shows good results.

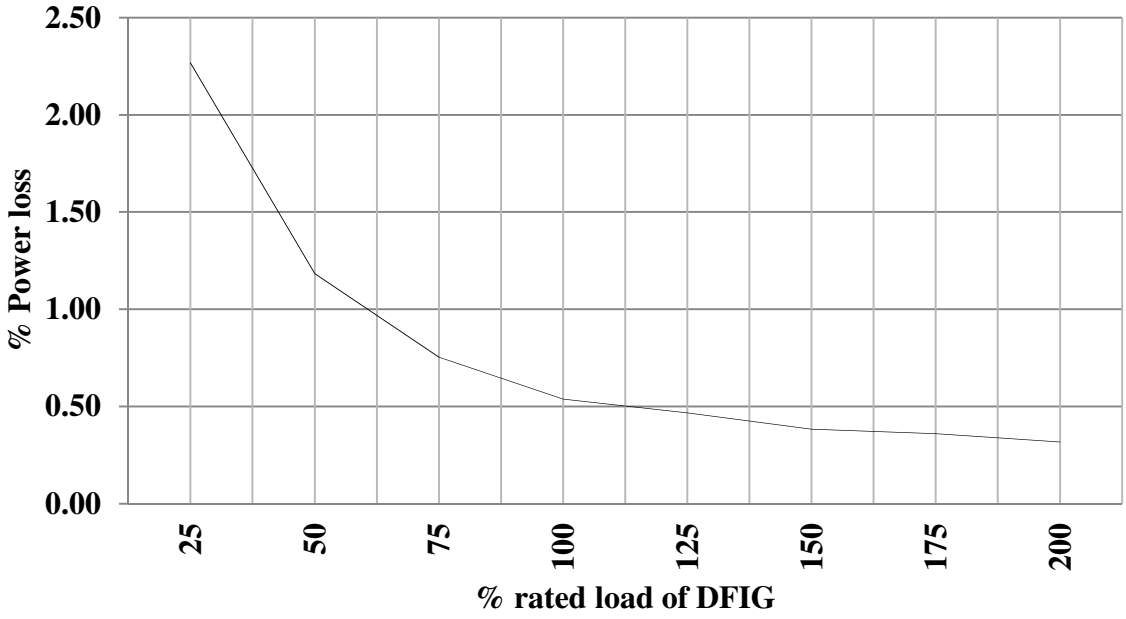

Fig. 6.4. Power loss (%) vs. Rated load of DFIG (%), load at bus B25

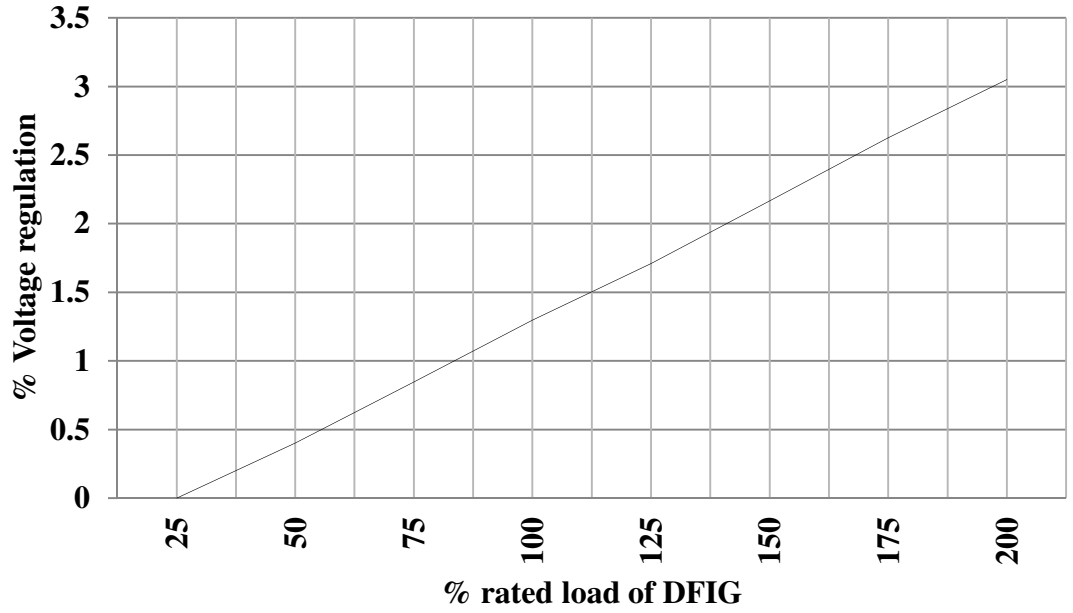

Fig. 6.5. Voltage regulation (%) vs. Rated load of DFIG (%), load at bus B25

6.2 Protection Techniques during LVRT

An asymmetrical three phase to ground fault simulated at bus B25, which is known as point of common coupling (PCC). Fault is initiated at t= 10 s and cleared at t= 10.1 s. The DC-link voltage is set at 1150 V. A resistive load of 1.5 MW is connected at bus B575. Threshold value for the DC bus voltage and rotor circuit current are set at 1800 V and 1.5 p.u. respectively. Three cases are considered to study dynamic performance of DFIG during LVRT. These three cases are without any protection, with crowbar protection and DC chopper protection.

6.2.1 Without Any Protection

A three phase to ground fault is initiated for 100 ms at the PCC without activating any protection. During fault back-to-back converter of DFIG are controlled to feed reactive power to the grid till system is not recovered. As shown in Fig. 6.6 PCC voltage is reduced to zero during fault for the time duration of 10 s to 10.1 s. Fig. 6.7 depicts that the stator voltage is reduced to 0.1 p.u. for the same duration of 10 s to 10.1 s.

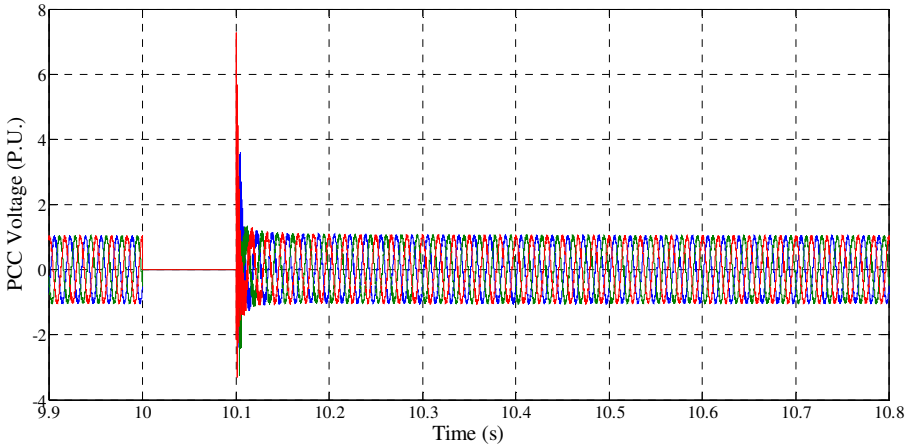

Fig. 6.6. PCC voltage reduced to zero

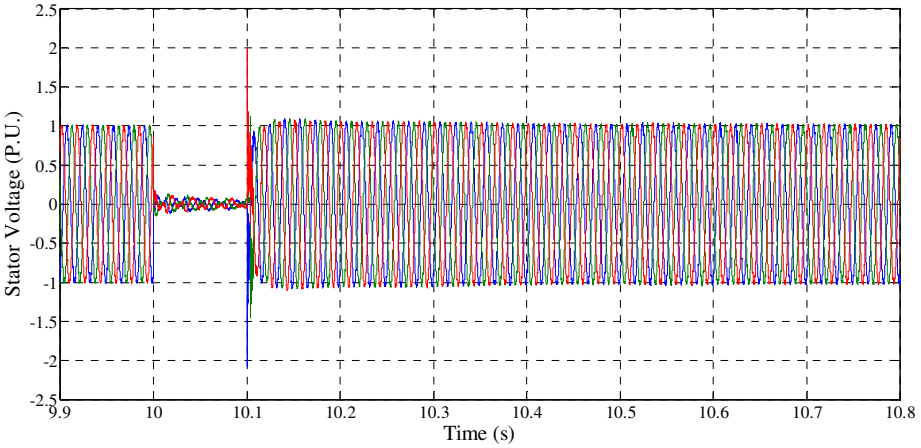

Fig. 6.7. Three phase to ground fault 0.9 voltage dip at stator voltage

During fault active power is zero for the duration of 10.01 s to 10.1 s and DFIG is controlled to feed reactive power to the system shown in Fig. 6.8, 6.9. Reactive power demand increased to limit DC-link voltage within limits.

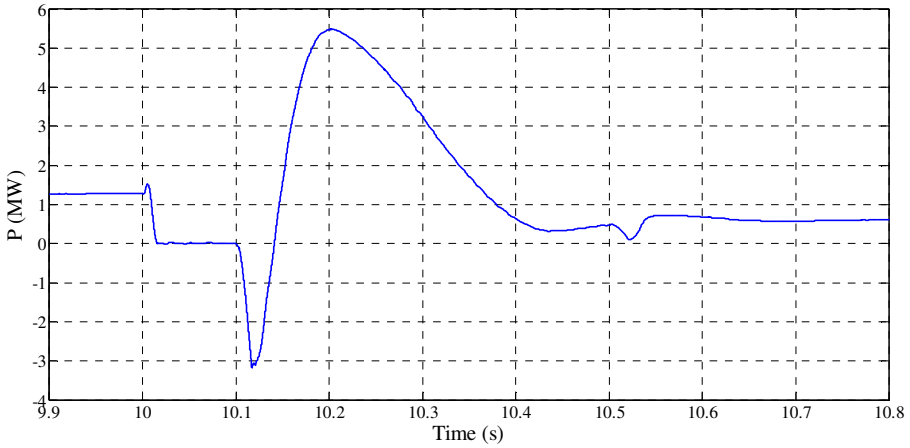

Fig. 6.8. Active power fed to PCC from WECS

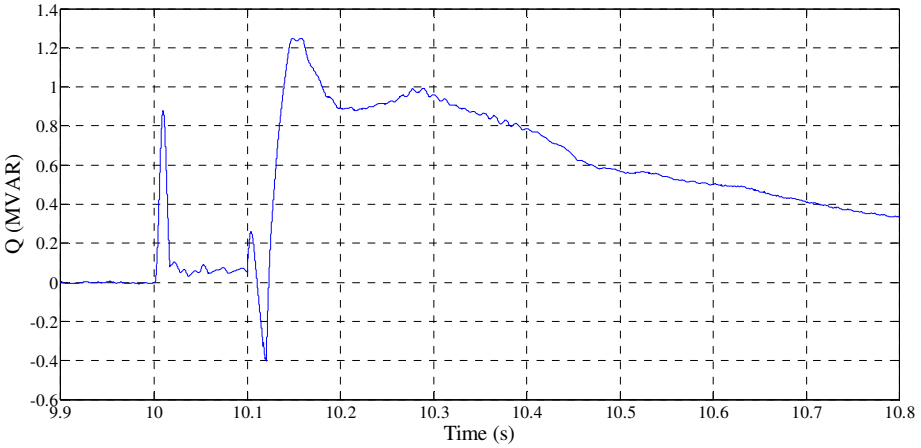

Fig. 6.9. Reactive power fed to PCC from WECS

DC-link voltage exceeds the nominal value of 1150 V and reaches the peak value of 1917 V at 10.03 s during fault as illustrated in Fig. 6.10. A very high value of 1649.5 V is observed at 10.52 s due to transient effect after which the value of V_{dc} is restored to initial value of 1150.

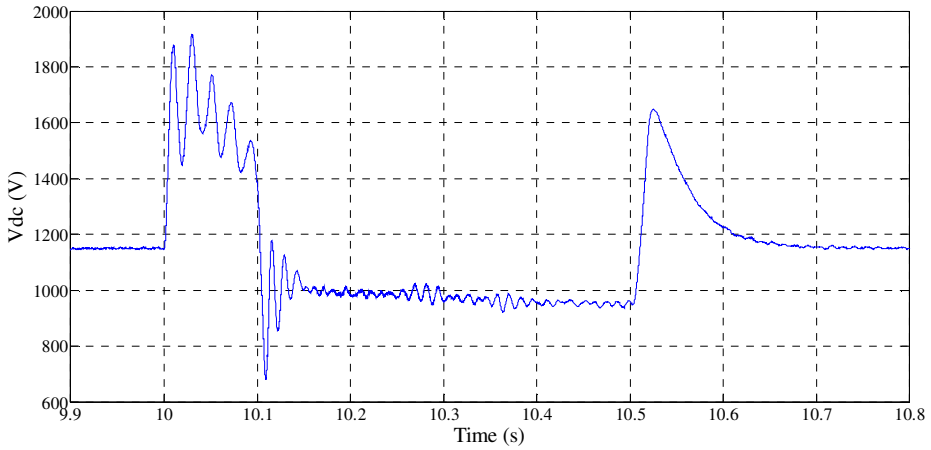

Fig. 6.10. DC-link voltage during fault

The rotor current peak value is 3.216 p.u. at 10.02 s which is more than double of the nominal value as portrayed in Fig. 6.11.

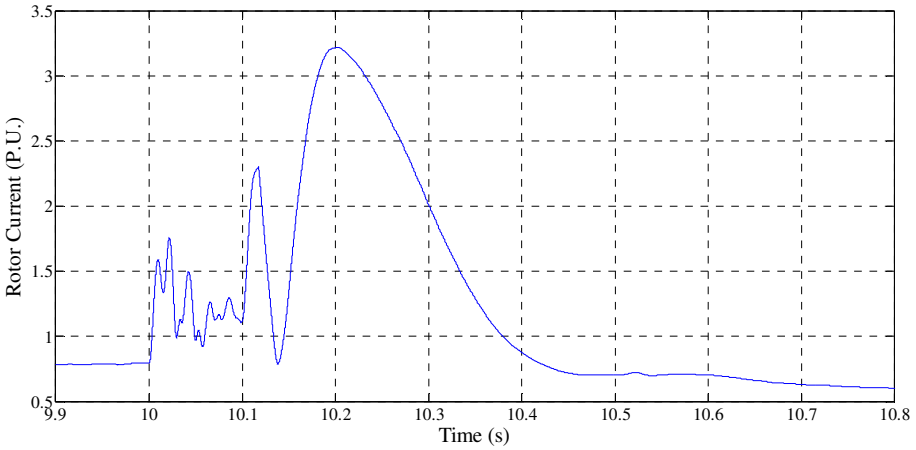

Fig. 6.11. Rotor current during fault

6.2.2. With Crowbar Protection

A crowbar circuit used to limit rotor circuit current and DC bus voltage during fault at bus B25. Active Crowbar is linked between RSC and rotor of DFIG. When fault occurred at the grid terminal crowbar bypass high transient rotor current due to voltage dip at the gird, where RSC is disabled. As illustrated in Fig. 6.12 crowbar circuit is made up of Diode Bridge connected to resistance through switch. Proposed crowbar control illustrated in Fig. 6.13. The proposed

control activates crowbar circuit and deactivates RSC if rotor current i_r, exceeds the threshold value of i_{rth} or if DC-link voltage V_{dc} exceeds threshold value of V_{dcth}.

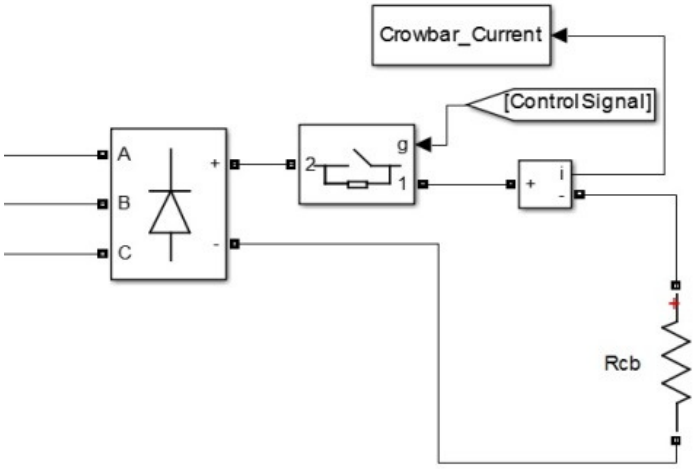

Fig. 6.12. Crowbar circuit [35]

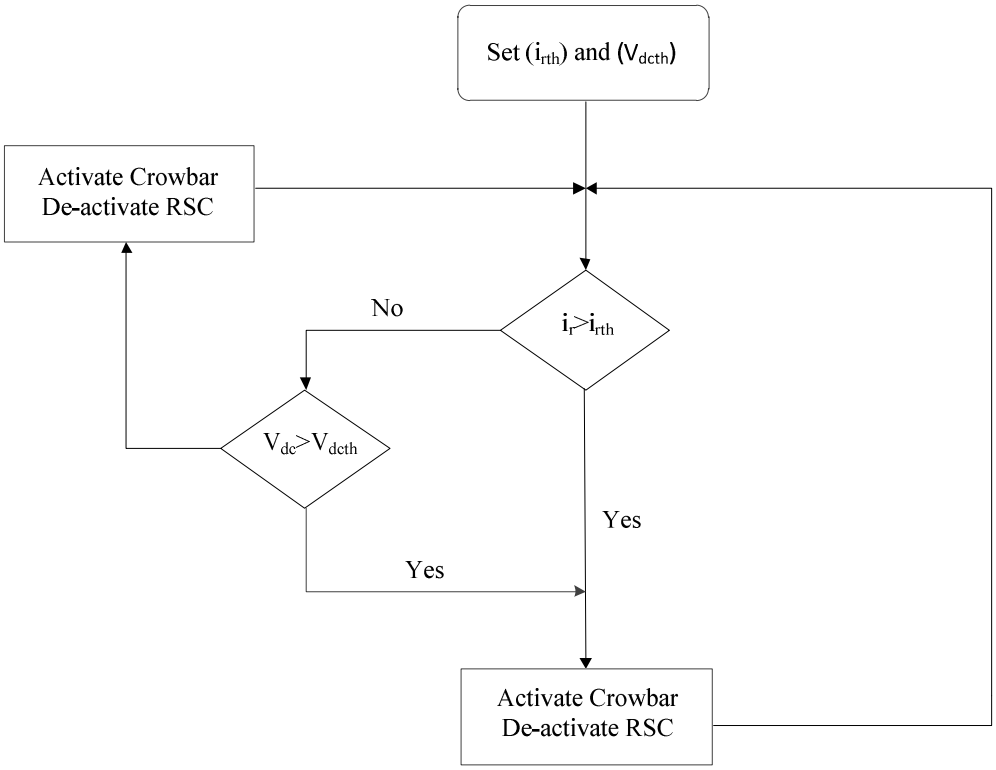

Fig. 6.13. Active crowbar control flowchart [35]

6.2.3 DC Chopper Protection

DC chopper circuits consist of power resistor connected in parallel to DC capacitor through power switch. When DC bus voltage or rotor circuit current exceeds their prescribed limit DC chopper circuit is enabled while RSC is still connected to the system. As illustrated in Fig. 6.14, DC chopper circuit is made up of resistor in series with the switching device.

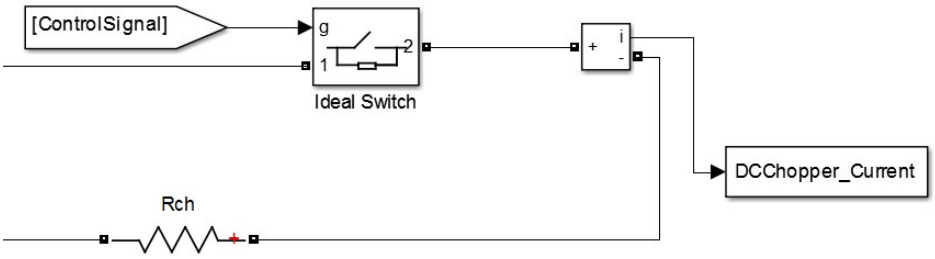

Fig. 6.14. DC chopper circuit

Choice of DC chopper resistance is important. Resistance value should be small enough to avoid large voltage at converter terminals and it should be high enough to limit DC bus voltage and rotor current within limits.

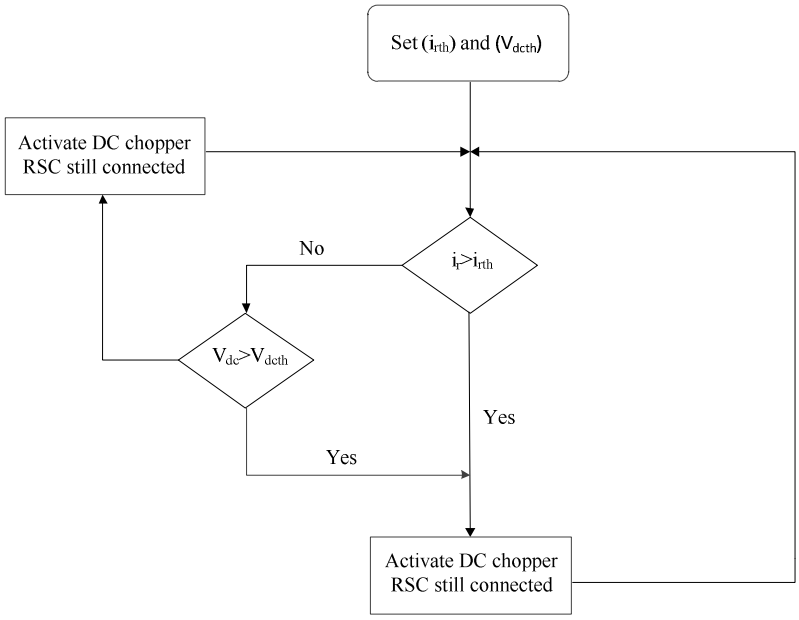

Fig. 6.15. DC chopper control flowchart

Proposed control scheme is illustrated in Fig. 6.15 for DC chopper control. The proposed control scheme is activates the DC chopper circuit but RSC is still connected to the system, if rotor current i_r, exceed the threshold value i_{rth}, or if the DC-link voltage, V_{dc}, exceeds the threshold value, V_{dcth}.

Three phase to ground fault is simulated to system for the duration of 100 ms and dynamic behavior of the system is analyzed without any protection, with activating the DC chopper and crowbar.

For the comparison purpose crowbar resistance and DC chopper resistance is taken as 0.001 ohm.

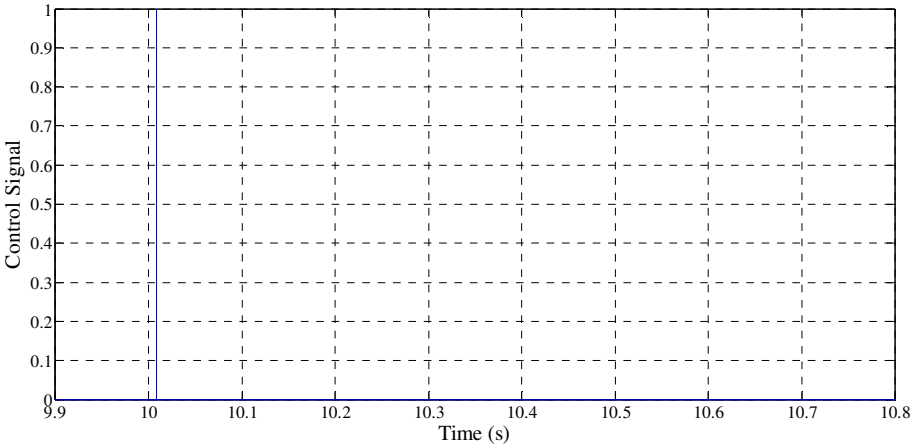

Fig. 6.16. Control signal

The Fig. 6.16 shows the control signal at 10.01 s, which is produced when DC bus voltage exceeds the limit of 1800 V for the activation of protection circuit. Fig. 6.17 portrayed current through the crowbar resistance having a value of 447 kA and Fig. 6.18 shows the current in DC chopper resistance is 740 kA.

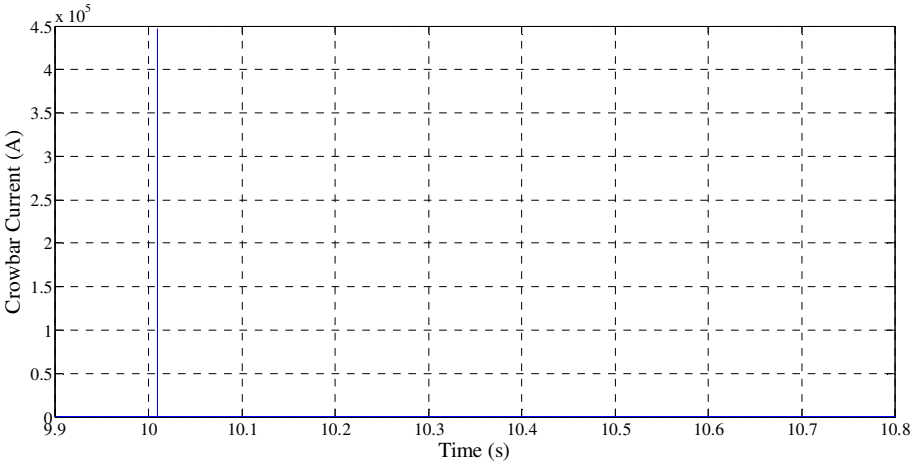

Fig. 6.17. Crowbar current

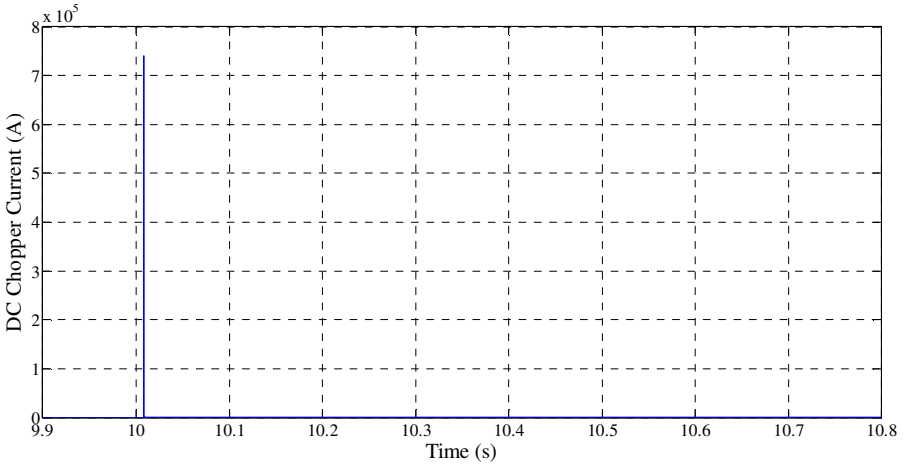

Fig. 6.18. DC chopper current

Fig. 6.19-6.24 show the comparative analysis between without any protection is represented by red color, with crowbar protection represented by green and with DC chopper protection is represented by blue.

Fig. 6.19-6.20 illustrates that the recovery period is increased in case of DC chopper, in blue color, as compared with the crowbar circuit, in green color, and without any protection, in red color, because in case of DC chopper reactive power drawn by the system is increased to limit DC-link voltage. Peak value of active power supplied by the DFIG based WT after clearance of

fault, in case of without any fault, with crowbar and with DC chopper are 5.48 MW, 5.45 MW is 5.35 MW respectively as shown in Fig. 6.19. Maximum value of reactive power after fault clearance in all three case without any protection, with crowbar and with DC chopper are 1.25 MVAR, 1.37 MVAR and 1.39 MVAR respectively as portrayed in Fig. 6.20.

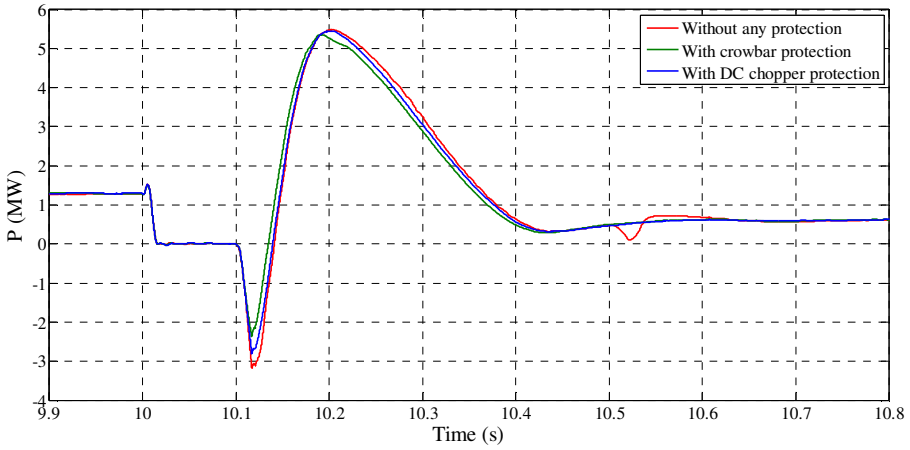

Fig. 6.19. Active power fed to PCC from WECS

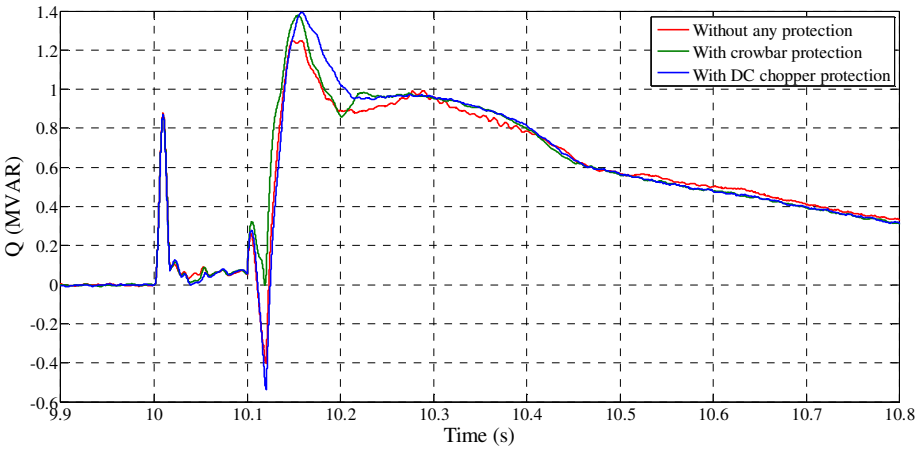

Fig. 6.20. Reactive power fed to PCC from WECS

Fig. 6.21 portrayed that transient in DC-link voltage is decreased more in case of DC chopper protection scheme shown in blue color as DC chopper resistance and crowbar resistance is taken as same and crowbar current is less than the DC chopper current as shown in Fig. 17, 18. Thus more voltage drop of transient in case of DC chopper as compare with the crowbar circuit. DC-link voltage after the transient are over in without any protection, with crowbar protection

and DC chopper protection are 1650 V, 1210 V and 1200 V respectively.

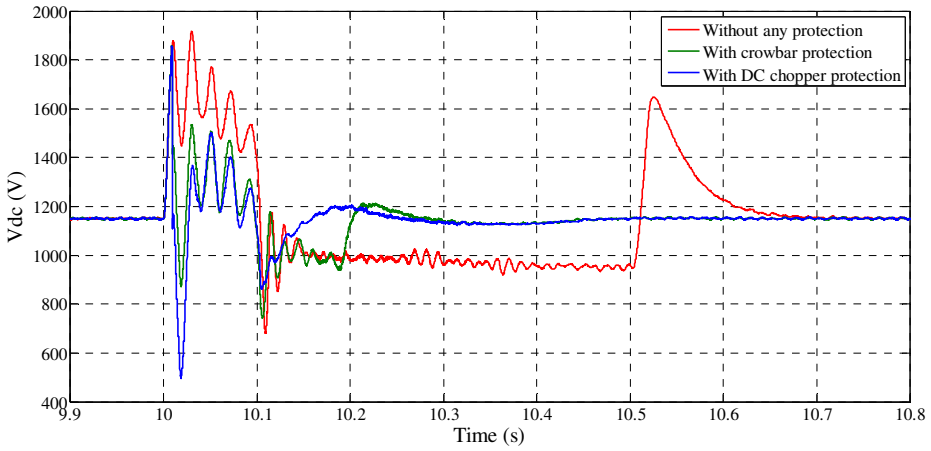

Fig. 6.21. DC-link voltage

Transient in rotor current are damped more in crowbar protection scheme, in green color, as represented in Fig. 6.22. Maximum value of rotor current in case of without protection is 3.216 p.u., crowbar circuit 3.18 p.u. and for DC chopper protection 3.207 p.u. As the stator and rotor circuit are coupled, due to voltage dip in the stator voltage, rotor current increase unexpectedly. As stator voltage is more improved during fault condition so the transient in the rotor current, for the case of crowbar circuit as compared with the case of without protection and with DC chopper circuit are less.

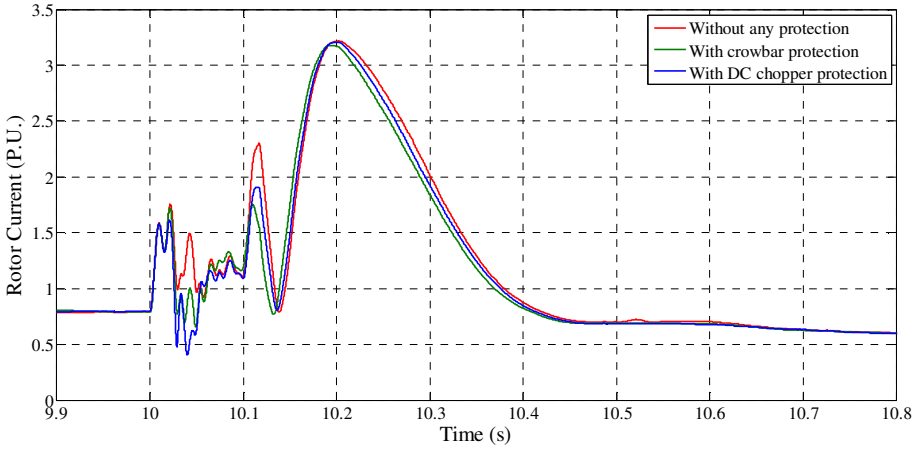

Fig. 6.22. Rotor current

The acceleration of the generator rotor with DC chopper protection is faster than crowbar protection as electromagnetic torque is more in case of DC chopper protection scheme, during the fault condition. Generator rotor speed for without any protection, with crowbar protection and for DC chopper protection are 1.145 p.u., 1.143 p.u. and 1.142 p.u. respectively as presented in Fig. 6.24. Electromagnetic torques for without any protection 2.1 p.u., for the crowbar circuit it is 1.67 p.u. and for DC chopper protection is 1.8 p.u. after fault clearance at 10.1 s as illustrated in Fig 6.23.

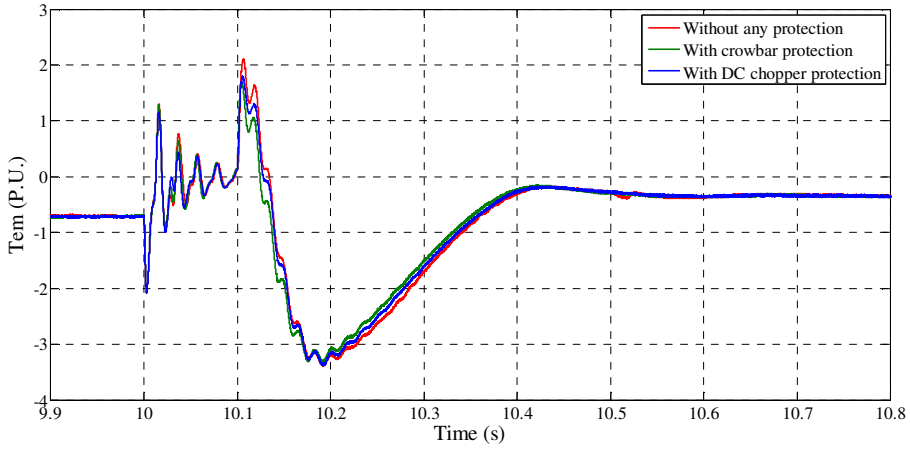

Fig. 6.23. Electromagnetic Torque

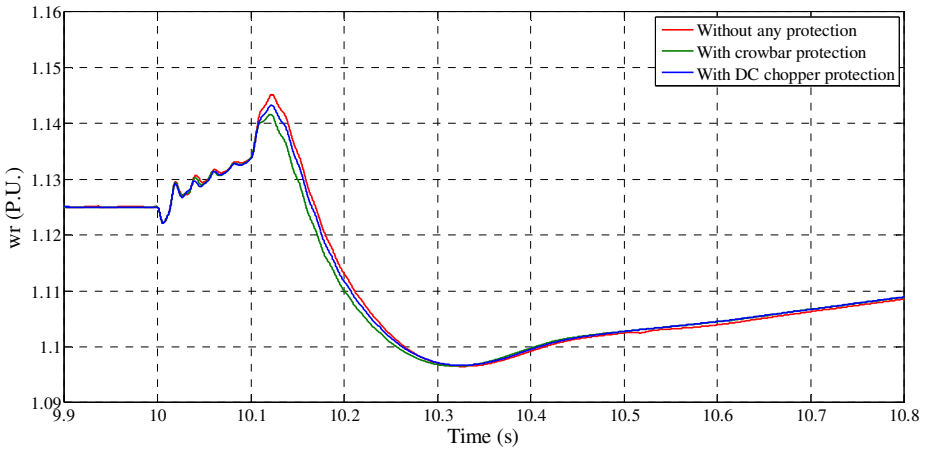

Fig. 6.24. Generator rotor speed

CHAPTER-7

CONCLUSION & FUTURE SCOPE OF RESEARCH

7.1 Conclusion

The presented work is mainly about study of voltage regulation and power loss as electrical load is increased from below rated to above rated capacity of DFIG. Moreover, a comparison is carried out between crowbar protection scheme and DC chopper protection scheme during an asymmetrical three phase to ground fault, when DFIG based WT is connected to grid supplying a resistive load of 1.5 MW. For comparison of dynamic behavior of DFIG based WT system value of crowbar resistance and chopper resistance is taken same. The salient contribution of the present work is the study of dynamic behavior of DFIG based WT under varying loading condition at different locations along the transmission line. The simulation results for loading conditions found satisfactory on the basis of voltage regulation and power loss obtained within satisfactory range. Another contribution of this paper is the study of LVRT capability of proposed system through implementation crowbar and DC chopper based protection system for DFIG under severe fault condition. The simulation results obtained for this part of study is found acceptable on the basis of the value of DC bus voltage, rotor current, real power and reactive power. The simulation method applied using MATLAB-SimPowerSystem software is highly recommended to investigate the performance of a DFIG based WT system at the stage of research and development to justify the robustness of the proposed system, reducing the R&D cost prior to onsite installation of the real system.

7.2 Future Scope of Research

The scope of work after studying and analyzing the DFIG based WT system is identified as:

i. The effect of inductive and capacitive loads on the dynamic behavior of proposed system during severe fault condition may be explored in future based on the outcome of present research work.
ii. In the near future, Application of Series dynamic braking resistor (SDBR) to the proposed model can be implemented and carry a dynamic behavior study of WECS.

BIBLIOGRAPHY

[1] T. Burton, E. Bossanyi, N. Jenkins, and D. Sharpe, "Introduction," in *Wind Energy Handbook,* 2nd edition, United Kingdom: Wiley, 2011, pp. 1-2.

[2] R. Datta and V. T. Ranganathan, "Variable-speed wind power generation using doubly fed wound rotor induction machine-a comparison with alternative schemes," *IEEE Transactions on Energy Conversion*, vol. 17, no. 3, pp. 414–421, 2002.

[3] V. C. Ganti, B. Singh, S. K. Aggarwal, and T. C. Kandpal, "DFIG-based wind power conversion with grid power leveling for reduced gusts," *IEEE Transactions on Sustainable Energy*, vol. 3, no. 1, pp. 12–20, 2012.

[4] F. Blaabjerg, Z. Chen, and T. Sun, "Voltage recovery of grid-connected wind turbines with DFIG after a short-circuit fault," *35th Annual IEEE Conference on Power Electronics Specialists,* vol. 3, 2004.

[5] C. D. Barker, and C. Zhan, "Fault ride-through capability investigation of a doubly-fed induction generator with an additional series-connected voltage source converter," *8th IEE International Conference on AC and DC Power Transmission,* pp. 79-84, 2006.

[6] Z. Peng, and H. Yikang, "Control strategy of an active crowbar for DFIG based wind turbine under grid voltage dips*," IEEE International Conference on Electrical Machines and Systems,* pp. 259-264, 2007.

[7] A. H. Kasem, E. F. El-Saadany, H. H. El-Tamaly, and M. A. Wahab, "A new fault ride-through strategy for doubly fed wind-power induction generator," *IEEE Conference on Electrical Power,* pp. 1–7, 2007.

[8] J. Vieira, M.N. Nunes, and U.H. Bezerra, "Design of optimal PI controllers for doubly fed induction generators in wind turbines using genetic algorithm," *IEEE Conference on Power and Energy Society General Meeting - Conversion and Delivery of Electrical Energy in the 21st Century*, pp.1-7, 2008.

[9] W. Z. W. Zhang, P. Z. P. Zhou, and Y. H. Y. He, "Analysis of the by-pass resistance of an active crowbar for doubly-fed induction generator based wind turbines under grid faults," *IEEE International Conference on Electrical Machines and Systems*, pp. 2316–2321, 2008.

[10] O. Anaya-Lara, Z. Liu, G. Quinonez-Varela, and J. R. McDonald, "Optimal DFIG crowbar resistor design under different controllers during grid faults," *3rd IEEE International Conference on Electric Utility Deregulation and Restructuring and Power Technologies,* pp. 2580–2585, 2008.

[11] P. Zhou, Y. He, D. Sun, and J. Zhu, "Control and protection of a DFIG-based wind turbine under unbalanced grid voltage dips," *IEEE Conference on Industry Applications Society Annual Meeting,* pp. 1–8, 2008.

[12] D. Li and H. Zhang, "A combined protection and control strategy to enhance the LVRT capability of a wind turbine driven by DFIG," *2nd IEEE International Symposium on Power Electronics for Distributed Generation Systems, pp*. 703–707, 2010.

[13] H. A. H. Aoyang, Z. Z. Z. Zhe, and Y. X. Y. Xianggen, "The impacts of distributed doubly-fed induction generators on smart distribution Grid protection," *IEEE International Conference on Modeling, Identification and Control,* pp. 71–75, 2010.

[14] C. Jin and P. Wang, "Enhancement of low voltage ride-through capability for wind turbine driven DFIG with active crowbar and battery energy storage system," *IEEE Conference on Power and Energy Society General Meeting,* pp.1-8, 2010.

[15] K. E. Okedu, S. M. Muyeen, R. Takahashi, and J. Tamura, "Comparative study between two protection schemes for DFIG-based wind generator," *IEEE International Conference on Electrical Machines and Systems,* pp. 62-67, 2010.

[16] W. Qiao, G. K. Venayagamoorthy, S. Member, and R. G. Harley, "Real-Time Implementation of a STATCOM on a Wind Farm Equipped With Doubly Fed Induction

Generators," *IEEE Transactions on Industry Applications*, vol. 45, no. 1, pp. 98–107, 2009.

[17] K. E. Okedu, S. M. Muyeen, R. Takahashi, and J. Tamura, "Protection schemes for DFIG considering rotor current and DC-link voltage," *IEEE International Conference on Electrical Machines and Systems,* pp. 2–7, 2011.

[18] K. E. Okedu, S. M. Muyeen, R. Takahashi, and J. Tamura, "Wind farms fault ride through using DFIG with new protection scheme," *IEEE Transactions on Sustainable Energy,* vol. 3, no. 2, pp. 242–254, 2012.

[19] L. Yang, Z. Xu, J. Østergaard, Z. Y. Dong, and K. P. Wong, "Advanced control strategy of DFIG wind turbines for power system fault ride through," *IEEE Transactions on Power Systems,* vol. 27, no. 2, pp. 713–722, 2012.

[20] M. Hongwei, X. Lie, and L. Yongdong, "Direct Power Control of DFIG Wind Turbines for Low Voltage Ride-Through," *7th IEEE International Conference on Power Electronics and Motion Control,* Vol. 3, pp. 2224–2227, 2012.

[21] S. Chandrasekaran, C. Rossi, D. Casadei, and A. Tani, "Improved control strategy of wind turbine with DFIG for Low Voltage Ride Through capability," *IEEE International Symposium on Power Electronics, Electrical Drives, Automation and Motion,* pp. 19–24, 2012.

[22] M. Wang, W. Xu, H. Jia, and X. Yu, "A new control system to strengthen the LVRT capacity of DFIG based on both crowbar and DC chopper circuits," *IEEE Conference on Innovative Smart Grid Technologies – Asia,* pp. 1–6, 2012.

[23] M. Z. Sujod and I. Erlich, "A new protection scheme for three-level NPC converter based DFIG using zero state control," *4th IEEE/PES Conference on Innovative Smart Grid Technologies Europe,* pp. 1–5, 2013.

[24] S. Abulanwar, Z. Chen, and F Iov, "Enhanced LVRT control strategy for DFIG-based WECS in weak grid," *IEEE International Conference on Renewable Energy Research and Applications,* pp. 476-481, 2013.

[25] P. Huang, M. Shawky, E. Moursi, S. A. Hasen, and S. Member, "Novel Fault Ride-Through Scheme and Control Strategy for Doubly Fed Induction Generator-Based Wind Turbine," *IEEE Transactions on Energy Conversion*, vol. 30, no. 2, pp. 635–645, 2015.

[26] M. M. Hussein, T. Senjyu, M. Orabi, M.A. Wahab, & M.M. Hamada, "Control of a variable speed standalone wind energy supply system," *IEEE Conference on Power and Energy,* pp. 71-76, 2012.

[27] O. Anaya-Lara, N. Jenkins, J. Ekanayake, P. Cartwright and M. Hughes, "Electricity Generation from Wind Energy," in *Wind Energy Generation: Modelling and Control*, 1st edition, United Kingdom: Wiley, 2009, pp. 1-17.

[28] Eoliennes Wind Farm. Available at http://www.michellehenry.fr. Accessed 18 February 2015

[29] Continental Wind Power. Available at http://www.continentalwindpower.com. Accessed 9 March 2015.

[30] M. Wang, W. Xu, J. Hongjie, and X. Yu(2012, May), "A new control system to strengthen the LVRT capacity of DFIG based on both crowbar and DC chopper circuits," *IEEE Conference on Innovative Smart Grid Technologies,* pp. 1-6, 2012.

[31] R. Gagnon, G. Turmel, C. Larose, J. Brochu, G. Sybille, and M. Fecteau, "Large-Scale Real-Time Simulation of Wind Power Plants into Hydro-Québec Power System," *Ninth International Workshop on Large-scale Integration of Wind Power into Power Systems as well as on Transmission Networks for Offshore Wind Plants,* Quebec City, Canada, *2010.*

[32] N. Y. Abed, M. M. Kabsha, and G. M. Abdlsalam, "Low Voltage Ride-Through protection techniques for DFIG wind generator," *IEEE Conference on Power and Energy Society General Meeting,* pp. 1-6, 2013.

[33] I. Erlich, S. Member, J. Kretschmann, J. Fortmann, S. Mueller-engelhardt, and H. Wrede, "Modeling of Wind Turbines Based on Doubly-Fed Induction Generators for Power System Stability Studies," *IEEE Transactions on Power System,* vol. 22, no. 3, pp. 909–919, 2007.

[34] N. W. Miller, W. W. Price, and J. J. Sanchez-gasca, "Dynamic modeling of GE 1.5 and 3.6 MW wind turbine-generators for stability simulations," *IEEE WTG Modeling Panel on GE Power Systems Energy Consulting*, 2003.," *GE-Power Systems Energy Consulting*, 2003.

[35] H. Soliman, M. Marei, R. M. El-Sharkawy, and K. M. El-Bahrawy, "Analysis of the dynamic behavior of a DFIG during grid disturbances using active crowbar protection," *12th IEEE International Conference on Environment and Electrical Engineering,* pp. 160-163, 2013.